WATER RESOURCES RESEARCH, VOL. 44, W01404, doi:10.1029/2006WR005643, 2008

Fate and transport of pathogens in a fractured aquifer in the Salento area, Italy

Costantino Masciopinto,[1] Rosanna La Mantia,[1] and Constantinos V. Chrysikopoulos[2]

Received 23 October 2006; revised 13 June 2007; accepted 26 September 2007; published 3 January 2008.

[1] This study investigates the fate and transport of pathogens introduced by artificial groundwater recharge at the Nardò fractured aquifer in the Salento area, Italy. Wastewater effluents from a municipal treatment plant with known pathogen concentrations were injected into a sinkhole and the migration of pathogens in the fractured aquifer was monitored at six sampling wells. The fate of pathogens was quantified by a mathematical model describing colloid transport in a set of three-dimensional, parallel fractures with spatially variable aperture. The number of parallel fractures and their average fracture aperture were determined from appropriate field pumping and tracer tests. The aperture spatial distribution was described by an experimental semivariogram developed from available field data obtained from two tracer tests and 34 pumping tests. The experimental results suggest that for the municipal wastewater injected into the Nardò aquifer the required most conservative set back distance for drinking wells should be over 8000 m.

Citation: Masciopinto, C., R. La Mantia, and C. V. Chrysikopoulos (2008), Fate and transport of pathogens in a fractured aquifer in the Salento area, Italy, *Water Resour. Res.*, *44*, W01404, doi:10.1029/2006WR005643.

1. Introduction

[2] In Mediterranean coastal semi-arid regions, partially treated municipal wastewater is often injected directly into sinkholes for artificial aquifer recharge and prevention of possible seawater intrusion. The Nardò aquifer in the Salento area, Italy (see Figure 1) receives only 650 mm of rainfall per year. Furthermore, during periods of drought there is a considerable reduction in groundwater storage due to excessive pumping and significant deterioration in groundwater quality due to landward migration of seawater [*Masciopinto and Carrieri*, 2002]. It should be noted that the Salento area receives over 70% of its fresh water supply from groundwater [*Regional Master Plan of Aqueducts*, 1998]. Prior to water distribution for human consumption, groundwater withdrawn from the aquifer in the Salento area is combined with surface water from local artificial lakes and the resulting mixture is chlorinated [*Masciopinto et al.*, 1999]. However, the possibility of surviving pathogens entering the distribution system may not be eliminated. Given that small concentrations of certain pathogens may cause serious illness in humans, e.g., gastroenteritis, hepatitis A, poliomyelitis [*Keswick and Gerba*, 1980], a careful assessment of the groundwater quality and a complete investigation of the mechanisms that govern the fate and transport of pathogens in the Nardò aquifer are required.

[3] To reduce the presence of pathogens to an acceptable level in the groundwater system of the Salento, safe distances between the sinkhole and the drinking water wells must be specified. Traditionally, mathematical models, treating pathogens either as finite particles (i.e., colloids) or as dissolved molecules, are used for preliminary estimation of pathogen movement in aquifers [*Chrysikopoulos and Sim*, 1996; *Schijven and Hassanizadeh*, 2000], and subsequent evaluation of setback distances [*Faulkner et al.*, 2003].

[4] Colloids present in subsurface formations are mainly mineral microparticles in the form of metal oxides, humic macromolecules, bacteria and viruses [*Stumm and Morgan*, 1981]. Colloids generally range in size from 1 nm to 10 μm; although, biocolloids such as bacteria range in size from 0.2 to 5 μm and they are much larger than dissolved contaminant molecules [*Chrysikopoulos and Sim*, 1996]. Consequently, the sorption of bacteria onto solids is described by colloid filtration theory [*Yao et al.*, 1971]. Viruses are at the lower end of the colloid size distribution with size ranging from 0.02 to 0.3 μm [*Brock and Madigan*, 1991]. Traditionally, the sorption of viruses behaving as solutes is represented by a nonequilibrium, first-order kinetic process [*Bales et al.*, 1991]; whereas, the sorption of viruses behaving as colloids can be described by colloid filtration theory [*Sim and Chrysikopoulos*, 1995; *Chrysikopoulos and James*, 2002].

[5] The fate and transport of viruses in subsurface formations are mainly governed by inactivation and sorption onto the solid matrix [*Vilker*, 1981; *Bales et al.*, 1989; *Sim and Chrysikopoulos*, 1995; *Ryan et al.*, 1999; *Jin et al.*, 2000]. Inactivation of liquid-phase as well as sorbed pathogens is an irreversible sink mechanism, commonly represented by a first-order expression [*Yates and Yates*, 1987; *Sim and Chrysikopoulos*, 1996]. Experimental data suggest that the inactivation rate is lower for attached than for liquid-phase pathogens [*Hurst et al.*, 1980; *Gerba*, 1984]. Furthermore, pathogen inactivation in subsurface formations is considerably affected by temperature [*Yates and Ouyang*, 1992]. It should be noted that viruses remain infective much longer at lower temperatures (1–8°C) than at higher temperatures (20–32°C) [*Park et al.*, 1992].

[1] Consiglio Nazionale delle Ricerche, Istituto di Ricerca sulle Acque Reparto di Chimica e Tecnologia delle Acque, Bari, Italy.
[2] Department of Civil Engineering, University of Patras, Patras, Greece.

0043-1397/08/2006WR005643$09.00

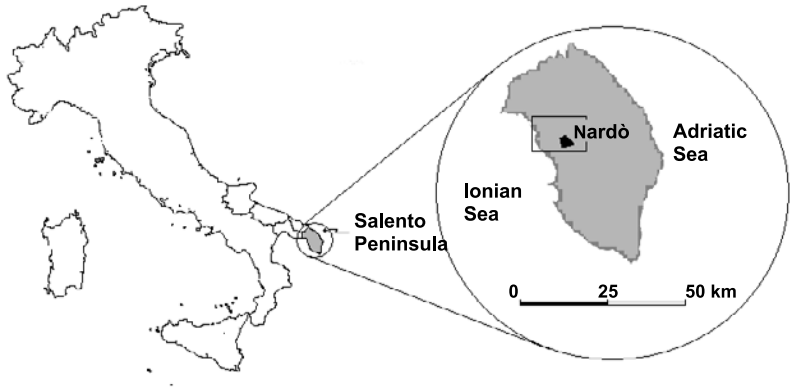

Figure 1. Map of the study area (Salento coast, Southern Italy).

[6] Several field-scale studies presented in the literature have been devoted to the investigation of colloid and pathogen migration [*McKay et al.*, 1993, 2000; *Kurosawa et al.*, 2006]. Analytical one-dimensional mathematical models [*Vilker et al.*, 1978; *Sim and Chrysikopoulos*, 1995; *Chrysikopoulos and Sim*, 1996], analytical three-dimensional models [*Sim and Chrysikopoulos*, 1998, 1999; *Anders and Chrysikopoulos*, 2005] and several numerical models [*Tim and Mostaghimi*, 1991; *Park et al.*, 1992; *Yates and Ouyang*, 1992; *Sim and Chrysikopoulos*, 1996; *Rehmann et al.*, 1999; *Bhattacharjee et al.*, 2002; *Schijven and Simunek*, 2002; *Faulkner et al.*, 2003] have been developed for the prediction of virus fate and transport in porous media. Numerous numerical models also have been presented in the literature for bacterial transport in porous media [*Harvey and Garabedian*, 1991; *Hornberger et al.*, 1992; *Jewett et al.*, 1995; *McCaulou et al.*, 1995; *Reddy and Ford*, 1996; *Unice and Logan*, 2000; *Zhang et al.*, 2001; *Mailloux et al.*, 2003]. Furthermore, the literature on colloid transport in fractured subsurface systems is extensive. Several analytical models have been developed for colloid transport in water saturated fractures using the relatively simple parallel plate model that represents a fracture as a pair of parallel plates separated by a constant aperture [*Abdel-Salam and Chrysikopoulos*, 1994; *James and Chrysikopoulos*, 2003a]. Moreover, numerous investigations explore the relatively complex case of colloid transport in fractures with spatially variable aperture [*Reimus*, 1995; *Chrysikopoulos and Abdel-Salam*, 1997; *James and Chrysikopoulos*, 2000; *Knapp et al.*, 2000; *James et al.*, 2005]. The majority of the available mathematical models describing colloid transport or contaminant/colloid co-transport in fractured systems assume that colloids are of uniform size [*van der Lee et al.*, 1992; *Smith and Degueldre*, 1993; *Abdel-Salam and Chrysikopoulos*, 1995a, 1995b; *Liu et al.*, 2000; *Oswald and Ibaraki*, 2001]. Colloids present in groundwater are known to follow a lognormal size distribution [*Ledin et al.*, 1994]. Consequently, recent numerical particle tracking and analytical models for colloid transport in fractures examine the realistic case of variably sized colloids [*James and Chrysikopoulos*, 1999, 2000, 2003b; *Chrysikopoulos and James*, 2002; *James et al.*, 2005].

[7] This study focuses on the fate and transport of various pathogens in the Nardò aquifer in the Salento area, Italy. The experimental data collected provide valuable information for appropriate setback distances of drinking wells from a designated sinkhole where secondary effluents from a municipal treatment plant are currently injected in order to prevent possible seawater intrusion.

2. Description of the Field Site

[8] The Nardò aquifer is located in the Salento Peninsula and it is approximately 8 km from the Ionian Sea coastline (see Figure 1). The formation of the Salento Peninsula consists mainly of sandstone, limestone and dolomite deposits. As illustrated in Figure 2, Miocene deposits known as Calcareniti di Gallipoli (sandstone), with layered thicknesses ranging from 5 to 7 m, are nearest to the ground surface. Below there is a formation of average thickness 30 m, consisting of Calcare di Altamura (limestone) intercalated by lenses of terra rossa (calcspar) and loamy sand. The underlying deposits are mainly limestone and dolomite. The water table is approximately 32 m below the ground surface. Freshwater floats over saline water originating from the Ionian Sea due to seawater intrusion.

[9] Hydrogeological studies of the Nardò aquifer show that the limestone rock formations are significantly fractured and very permeable. The rock fractures are interconnected and partly filled with calcspar or terra rossa. Groundwater flows along preferential pathways within the aquifer under a piezometric head approximately 3 m above the mean sea level. The preferential pathways are mainly horizontal conduits. The Miocene rock formations are also fractured but the interconnected fractures are orientated along the local bedding plans.

[10] The Nardò aquifer supplies fresh water to numerous households along the Ionian Sea coastline. Consequently, the water quality of the Nardò aquifer should be maintained continuously at acceptable levels. To monitor the water quality of the aquifer, seven sampling wells (Wells #1, #2, #3, #4, #5, WT1 and WT2 shown in Figure 3) were placed within a 3 km radius from the sinkhole. The sinkhole is a large hollowed-out place, similar to a vertical cave, having an estimated diameter of approximately 7 m. Table 1 lists water quality data from water samples collected during the winter of 1999. Furthermore, 70 m deep vertical profiles of groundwater salinity (g/L), groundwater temperature (T_e °C), and dissolved oxygen (DO) were obtained by immersion of the Ocean Seven probe (Idronaut S.r.l., model 401). As

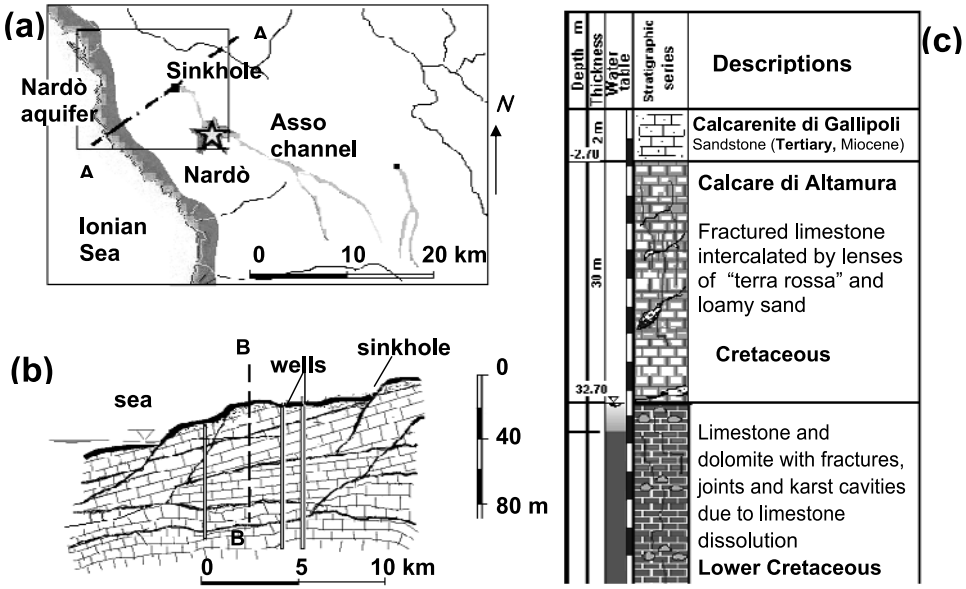

Figure 2. The Nardò fractured aquifer. (a) Plan view with location of the sinkhole. (b) Cross-section view along A-A. (c) Stratigraphic series along cross-section B-B.

shown in Figure 4, the groundwater salinity in Well #3 increased with depth below the water table from 0.35 g/L (at 0.2 m) to 0.54 g/L (at 35 m), the temperature varied from 14.9 to 15.5°C and the DO decreased from 6 to 4 mg/L. It should be noted that the injected water was at ambient temperature, which ranges from 5 to 12°C during the winter months. Disinfection by-products such as trihalomethanes (THM) and other volatile and non-volatile halo-organic compounds (TOX) were detected in numerous water samples. It should be noted that these contaminants are produced due to chlorination at the municipal treatment plant, and they are known to be carcinogens. The concentrations of heavy metals were generally below the Italian drinking water limits [*D. Lgs. 31/2*, 2001]. Several wells contained measurable amounts of dissolved organic carbon (DOC) and trace amounts of ammonia and nitrate. The presence of organic compounds as well as the elevated chloride concentrations due to seawater intrusion, prevented the use of

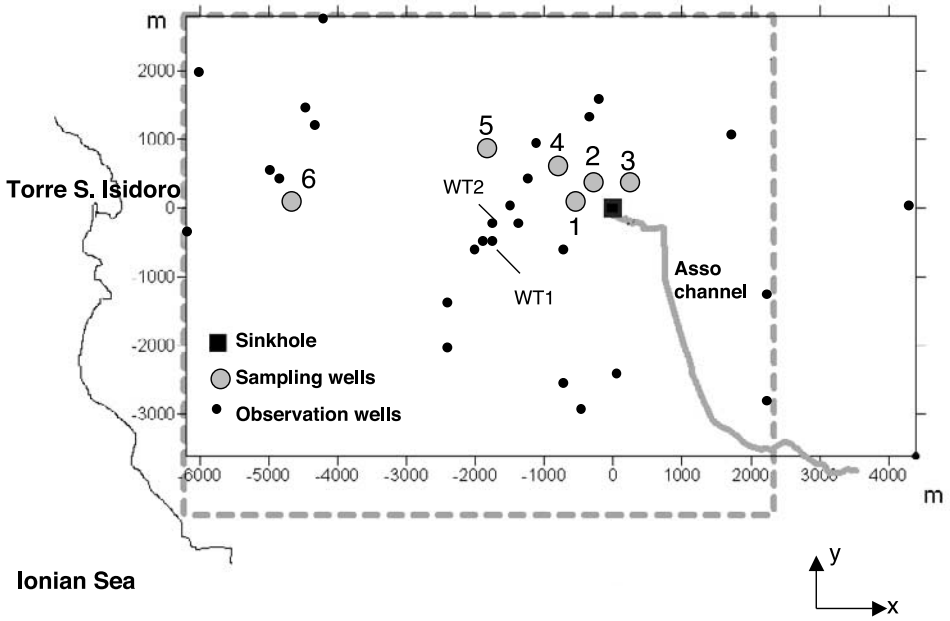

Figure 3. Field location of the sinkhole, sampling wells, and observation wells. The observation wells were used for the estimation of the mean fracture aperture (the broken line border shows the discretized domain for the computational procedure).

Table 1. Water Quality of the Injected Water and Groundwater in the Nardò Aquifer

	Injected Wastewater[a]	Groundwater[b]		
	Mean	Min.	Mean	Max.
SC (μS/cm)	400	220	877	3000
pH	7.75	6.5	7.3	7.9
Temperature, °C	17.8	14	15.4	17.7
N-NH_4^+, mg/L	Traces	0	0	Traces
N-NO_2^-, mg/L	0.03	0	0	0
N-NO_3^-, mg/L	8	0	6.8	18
Chloride, mg/L	61	14	115	402
DOC, mg/L	47	0	12	41
TOX (μg/L as Cl^-)	25.5	0	7	28

[a]Average from 15 samples.
[b]Average from 64 samples collected from 7 sampling wells.

groundwater for drinking purposes. Nevertheless, it should be noted that not all of the samples collected exceed the drinking water standards.

[11] During the period November 2001 to July 2003 the sinkhole and six sampling wells (see Figure 3) were monitored monthly for the presence of bacteria, *Escherichia coli*, *Clostridium perfringens (C.) spores*, *fecal coliforms*, *fecal streptococci*, and *somatic coliphages anti-Escherichia coli*. Note that Wells #1, #2 and #5 are located 320 m, 500 m, and 3 km from the sinkhole, respectively. Water samples were collected after 10 min of pumping to ensure that the stagnant water in the pipelines had been completely displaced. For monitoring wells without pumps, water samples were extracted at a flow rate of 1–2 L/min with a sampler (Grundfos S.r.l., model MP1) placed 0.5 to 1 m below the water table. During the sampling period, only minor water table and groundwater quality fluctuations were observed due to the relatively steady quality and quantity of the water injected into the sinkhole. The measured microbiological indicator levels are presented in Figure 5. Clearly, there is a strong dependence of groundwater quality on distance from the sinkhole. At a distance of 3 km from the sinkhole (Well #5), the concentrations of *C. spores* (Figure 5c) and somatic coliphages (Figure 5f) are approximately equal to background levels. It should be noted that both *C. spores* and *somatic coliphages* are considered good indicators of enteroviruses in water [*Payment and Franco*, 1993]. On the basis of most of the samples collected from Well #5 (see corresponding data for the period November 2001 to February 2002 in Figures 5a, 5b, and 5d) it is evident that the groundwater cannot be used for drinking without prior disinfection treatment because the values for total bacterial count, *Escherichia coli*, and *fecal coliforms* levels are above the Italian drinking water limits, which are set at 100 CFU/mL for total bacteria and zero counts for all other pathogens [*D. Lgs. 31/2*, 2001]. Furthermore, Figure 6 clearly shows that the averaged pathogen concentrations observed during the sampling period November 2001 to July 2003 in the sinkhole, Well #1, Well #2, Well #5, and Well #6 exceed the Italian drinking standards.

2.1. Field Tests

[12] For the mathematical modeling of groundwater flow and pathogen transport in the Nardò fractured aquifer several model parameters are required. Assuming that the aquifer can be conceptualized as a three-dimensional set of parallel fractures, the number of parallel fractures, their transmissivities, and the structure of the spatially variable fracture aperture must be determined from appropriate field tests. Consequently, two tracer tests and 34 pumping tests were conducted. The data from one of the pumping tests were fitted by the Thies solution for unsteady flow, whereas the remaining pumping tests were analyzed by the Thiem equation [*Bear*, 1979, p. 306]. The tracer tests were carried out during the Summer of 1982 using iodine and during the winter of 1999 using chlorophyll as conservative tracers. The iodine test was carried out at the injection-extraction well pair WT1-WT2. Both WT1 and WT2 are 50 m deep and they are located approximately 2 km from the sinkhole (see Figure 3). The chlorophyll single-well tracer (slug or borehole dilution) test was performed at Well #3. The drawdown-recovery pumping test was carried out at Well #4. Furtheremore, the well locations of the other 33 pumping tests are listed in Table 2.

2.1.1. Iodine Tracer Test

[13] The iodine ion (I^-), in the form of the moderately soluble sodium iodide salt (NaI), was chosen for the conservative inorganic tracer. Alkali halides are the most commonly used salts for subsurface fluid tracing [*Chrysikopoulos*, 1993]. Three different initial tracer concentrations (C_o = 217, 283, and 384 mg/L) were injected into well WT1. A 80 HP pump placed in well WT2 provided forced gradient conditions at three different flow rates (Q_w = 112, 50, and 25 m^3/h). Note that the separation distance between WT1 and WT2 is 11.7 m. The three initial I^- concentrations used were prepared by dissolving 35.7, 46.7, and 63.3 g of NaI (85% pure) in 8 liters of well water, respectively. Each 8-liter tracer solution was injected into the well column of WT1, which has a total volume of 132 liters. A uniform iodine concentration was maintained in the wellbore during the tracer test by continuously recycling the water in the wellbore with a 5 HP pump, at a rate of 10 m^3/h. The observed I^- breakthrough concentrations at WT2 for the three different flow rates are presented in Figure 7. Analysis of the

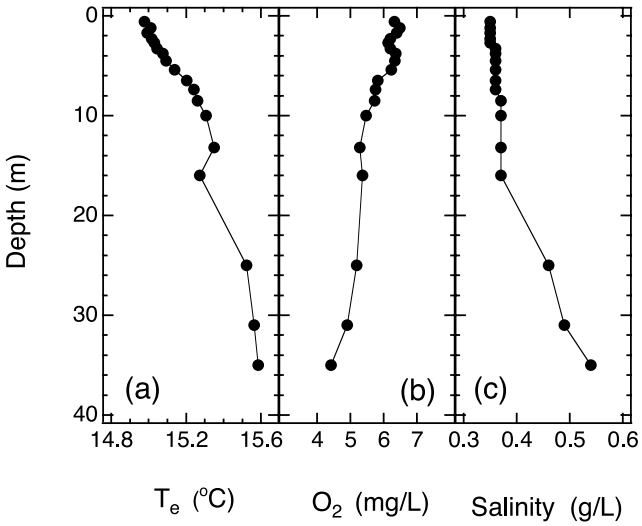

Figure 4. Vertical profiles in Well #3 during the winter of 1999 of (a) water temperature, (b) dissolved oxygen, and (c) water salinity.

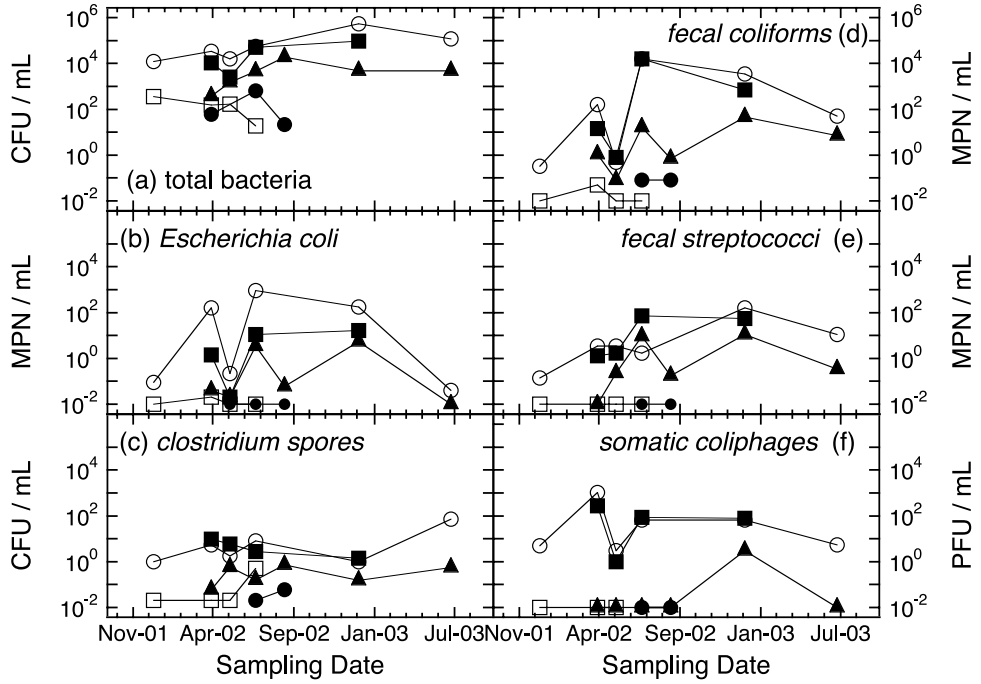

Figure 5. Observed (a) total bacterial count at 37°C; (b) *Escherichia coli*, (c) *Clostridium spore*s, (d) *fecal coliforms*, (e) *fecal streptococci*, and (f) *somatic coliphages anti-Escherichia coli* at the sinkhole (open circles), Well #1 (solid squares),Well #2 (solid triangles), Well # 5 (open squares) and Well #4 (solid circles, background values).

breakthrough curves indicates a low degree of tracer mixing in the fractures. The iodine tracer mass recovered at WT2 was 31.0 g (87%), 33.4 g (71.5%) and 25.8 g (41%), for each of the three flow rates (Q_w = 112, 50 and 25 m^3/h), respectively. The spreading of the tracer breakthrough curves is proportional to the dispersion coefficient [*Levenspiel*, 1972, p. 281]. Consequently, the low degree of tracer mixing suggests the presence of a fracture network without a substantial number of interconnections (parallel fractures). The shape of the extended tail of the tracer breakthrough curves shown in Figure 7 suggests that the various parallel conduits carried the injected water to WT2 at slightly different velocities.

[14] The sum of the various fracture apertures intersecting a vertical cross-section of the aquifer can be estimated by the following expression [*Masciopinto et al.*, 1997]:

$$\sum_{i=1}^{N_f} \hat{b}_i = \frac{Q_w t_p}{\pi\left(r^2 - r_w^2\right)} \tag{1}$$

where $\hat{b}_i$ (L) is the mean aperture of fracture i with spatially variable aperture, Q_W (L^3/t) is the pumping flow rate; t_p (t) is the pumping period; r_w (L) is the radius of the pumping well; r (L) is the radial coordinate distance from the pumping well, which for the present tracer test is the separation distance between injection-well WT1 and pumping-well WT2. The number of the horizontally oriented parallel fractures of the aquifer, N_f (-), can be determined by

$$N_f = \frac{1}{\bar{b}} \frac{Q_w t_p}{\pi\left(r^2 - r_w^2\right)} \tag{2}$$

where $\bar{b} = \left(\hat{b}_1 + \hat{b}_2 + \ldots + \hat{b}_i + \ldots + \hat{b}_{N_f}\right)/N_f$ is the average of the mean apertures of the parallel fractures, which can be estimated by [*Tsang*, 1992]:

$$\bar{b} = \left[\frac{6}{\Delta\phi t_p} \frac{\mu_w}{\gamma_w}\left(r^2 - r_w^2\right) \log\left(\frac{r}{r_w}\right)\right]^{1/2} \tag{3}$$

where $\Delta\phi$ (L) is the piezometric head difference between injection-well WT1 and pumping-well WT2; γ_w ($M/L^2 \cdot t^2$) is the specific weight of water; and μ_w (M/L · t) is the dynamic viscosity of water. Furthermore, the desired value of the aquifer effective porosity, n_e (-), can be estimated by dividing the sum of the fracture apertures as evaluated from (1) by the average saturated aquifer thickness, B, to yield:

$$n_e = \frac{1}{B} \sum_{i=1}^{N_f} \hat{b}_i \tag{4}$$

The pumping period, t_p, can be estimated directly from the experimental tracer breakthrough data (see Figure 7). The maximum observed tracer concentration arrives at the pumping well at a time equal to t_p. For the three breakthrough iodine tracer data sets collected in this study for Q_w = 112, 50 and 25 m^3/h, the observed drawdowns were $\Delta\phi$ = 12, 4.5 and 2 cm, respectively. Furthermore, the corresponding pumping periods, as shown in Figure 7, were estimated to be t_p = 12, 26 and 40 min, respectively. For the parameters r_w = 0.15 m, r = 11.7 m, B = 15 m, and μ_w/γ_w = 1.16×10^{-7} m · s for water at 15°C [*Weast*, 1969], (3) is employed to evaluate $\bar{b}$ = 1.98 ± 0.24 mm. Subsequently, (2) is used to obtain N_f = 24 ± 3, and (4) to obtain n_e = 0.0032 ± 0.0004. Note that the estimated confidence

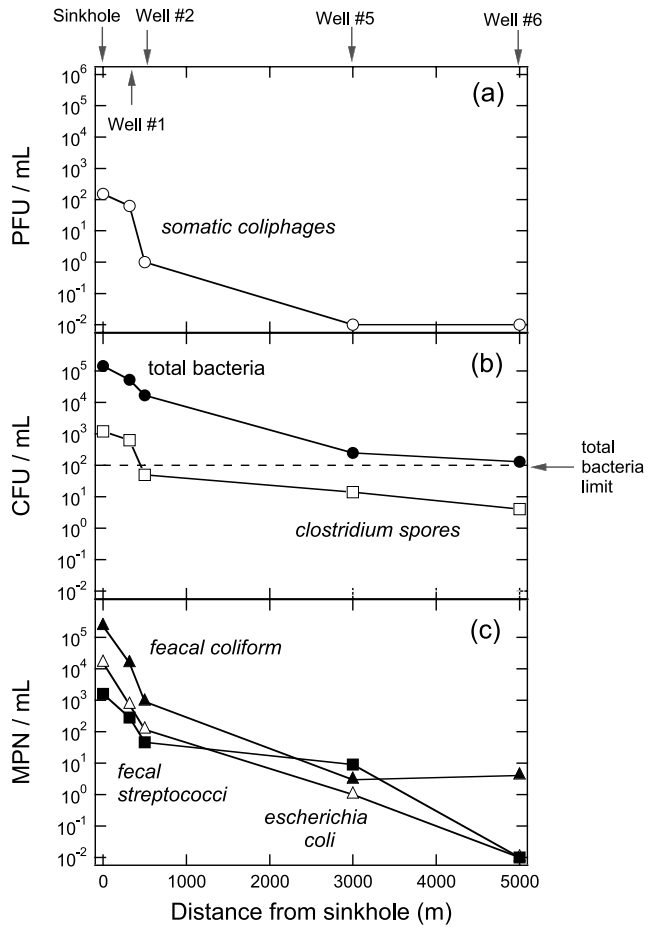

Figure 6. Average pathogen concentrations as a function of distance from the sinkhole for (a) *somatic coliphages*, (b) total bacteria and *clostridium spores*, and (c) *fecal coliforms, fecal streptococci and Escherichia coli*. The broken line indicates the drinking water regulations limit for total bacteria (100 CFU/mL).

intervals are the standard deviations of the average parameter values determined from the three different tracer tests.

2.1.2. Chlorophyll Borehole Dilution Tracer Test

[15] Accurate characterization of an aquifer requires that $\bar{b}$ is estimated at several field locations. Consequently, a chlorophyll tracer single-well test (borehole dilution test) was carried out to determine $\bar{b}$ for the vertical saturated aquifer thickness at Well #3, which is 70 m deep with radius r_w = 15 cm and is located 600 m from the sinkhole (see Figure 3). The water table elevation within Well #3 is 30 m below ground surface. Therefore the saturated aquifer is B = 40 m thick. Note that Well #3 was equipped with 8 samplers, 5 m apart, located below the water table to allow samples at different depths within the wellbore to be collected simultaneously.

[16] A special device consisting of flexible pipelines and a sequence of 7 stainless steel samplers, positioned 5 m apart, was placed in Well #3. The water filled portion of the well was divided with inflatable packers into 7 sections. Each section contained one sampler. Subsequently, a 2.5 g/L chlorophyll solution with specific conductance SC = 1.74 mS/cm, prepared with previously pumped water, was injected into the entire length of Well #3 at a rate of 30 m^3/h for approximately 6 min, using a plastic pipeline. A total of 2.5 m^3 of chlorophyll solution was injected. The water levels in the well were monitored during and after the chlorophyll solution injection for a period of 5 h in order to evaluate the unsteady radial water flow from Well #3. Compressed air at a low pressure (0.5 bar) was used to inflate all packers simultaneously. The inflated packers completely isolated 7 sections of the wellbore. Groundwater entered into each of the 5 m thick sections and diluted the chlorophyll concentration. During the first 24 h of the chlorophyll borehole dilution tracer test no water samples were collected to avoid possible errors due to density effects and sorption onto the borehole aquifer materials. After the 24 h delay period, water samples were collected simultaneously from each sampler every 30 min. The chlorophyll concentration of the first sample from each isolated section represents its initial chlorophyll concentration, C_o. All water samples were collected at a distance x = 1.5 cm away from the wellbore. This is the distance between the inlet port of the sampler and the borehole wall, which sustained the stainless steel samplers, as shown in Figure 8. The water samples were transported from each sampler to the ground surface through individual pipelines with a system utilizing compressed air at 6 bars. To eliminate the possibility of sample exposition to direct sunlight, all the water samples were placed in black 100 cm^3 bottles. Chlorophyll concentrations in the collected water samples were detected with a fluorometer (Turner Design mod. 10-AU) equipped with a flow-cell filter. The measured chlorophyll concentrations are shown in Figure 9 and indicate that the dilution within the wellbore is caused mainly by natural groundwater inflow.

[17] The theory of borehole dilution tests where a tracer is injected into a well-mixed isolated section of a borehole and the flow is pure convective has been thoroughly presented by *Palmer* [1993]. However, for the present dilution tracer test, where the water between the packers within the well is not mixed, the transport of chlorophyll between the wellbore wall (x = 0) and the location of the sampler (x = 1.5 cm) is governed by the following one-dimensional advection-dispersion partial differential equation

$$\frac{\partial C(t,x)}{\partial t} = D\frac{\partial^2 C(t,x)}{\partial x^2} - U\frac{\partial C(t,x)}{\partial x} \tag{5}$$

where U (L/t) is the water velocity or equivalently the specific discharge $q = U/n_e$ for $n_e = 1$; D (L^2/t) is the hydrodynamic dispersion coefficient of chlorophyll in the water; x (L) is the Cartesian coordinate along the direction of flow ($0 \le x \le 2r_w$); and t (t) is time. The appropriate initial and boundary conditions are:

$$C(0,x) = C_0 \tag{6a}$$

$$C(t,0) = C_b \tag{6b}$$

$$\frac{\partial C(t,2r_w)}{\partial x} = 0 \tag{6c}$$

Table 2. Well Coordinates and Measurements

Well Name	Well Coordinates x, m	Well Coordinates y, m	Water Table Depth Below the Ground, m	Piezometric Heads[a] ϕ (m Above Sea Level)	$Q_w/\Delta\phi$, L/s · m	B, m	$\bar{b}$, μm	$Y = \log_{10} \bar{b}$
Sinkhole	0	0	29.13	5.26	-	40	574	2.76
Masseria Li Manieli	2300	−1300	31.35	2.01	1	40	64	1.83
Masseria Auletta	−1700	−250	38.22	1.96	525	67	2459	3.41
Pozzo n. 6-82	−1200	350	35.27	1.21	350	40	2724	3.45
Pozzo n. 7-82	−1400	−200	36.42	1.14	500	22	2771	3.46
Pozzo n. 8-82	−1750	−400	37.98	1.10	500	30	2370	3.39
Pozzo n. 9-82	−2000	−650	38.05	1.10	667	41	2771	3.46
Pozzo n. 10-82	−750	−650	35.06	1.16	275	40	1780	3.27
Pozzo n. P-82	−1400	−200	36.54	1.02	65	40	660	2.84
Pozzo n. 14-82	0	−2400	33.88	0.98	125	69	1675	3.24
Pozzo n. 17-82	−650	−2600	36.29	0.94	280	21	2520	3.42
Pozzo n. 18-82	−550	−3000	35.55	0.94	900	20	3220	3.52
Masseria Li Monaci	2300	−2800	35.62	2.03	533	40	2713	3.45
Coltura	3214	−5288	38.53	1.37	65	33	993	3.01
10IIIS	8310	−4701	37	2.09	3	30	90	1.97
Villaggio Resta	−2400	−1350	25.37	0.65	4	155	222	2.36
Bonocore	4400	−3600	20.8	1.00	1	41	72	1.87
Masseria Termite	−1900	−450	41.1	0.70	40	53	1195	3.09
Masseria Builli	−4200	2800	32.96	-	700	13	2840	3.47
Masseria Olivastro	1800	1100	31.73	2.97	106	40	1628	3.23
Masseria Abatecola	−5947	2005	33.7	-	800	18	3036	3.50
Masseria Fachechi	−1100	900	39.11	1.37	165	40	2172	3.35
Masseria Pendinello	−4400	1500	42.43	1.77	26	16	1226	3.11
Masseria Termite	−1850	−500	40.82	0.98	48	8	1209	3.10
Masseria Messere	−4383	1136	37.86	1.76	300	15	1859	3.29
Masseria T. Termite 1	−4800	400	34.44	0.57	30	20	828	2.93
Masseria T. Termite 2	−4900	450	42.48	0.89	178	30	1652	3.24
Masseria Ascanio	−8954	6108	31.7	0.80	10	30	584	2.78
Masseria Torre Termite	−6200	−400	23.58	0.46	111	13	1431	3.17
Masseria Nanni	4400	50	41.07	2.44	210	25	1555	3.21
Masseria Molinari	10410	−1767	44.58	2.53	19	40	529	2.74
11RFBO	−19083	11451	60.1	1.39	23	31	725	2.88
22RFBO	−14296	11667	44.5	2.42	15	20	791	2.92
Well #3	0	420	31.05	3.2	-	30	330	2.52
Well #4	−500	430	33.40	2.6	70	30	1043	3.02
Pozzo Torre Termite 3	−4604	319	41	0.05	15	30	933	2.97
Well #1	−320	150	-	2.64	-	-	-	-
Well #2	−300	400	-	3.08	-	-	-	-
								$\bar{Y}$ = **3.03**

[a]Observed during the winter of 2002.

where t = 0 is the instant when the chlorophyll injection is completed; C_0 (M/L^3) is the initial aqueous phase chlorophyll concentration within the wellbore evaluated 24 h after the chlorophyll injection was completed, and C_b (M/L^3) is the background chlorophyll concentration in the groundwater. The analytical solution of the governing partial differential equation (5), subject to initial and boundary conditions (6a)–(6c), is well known and can be found in the tabulation by *van Genuchten and Alves* [1982, p.12]. The water velocity at various depths in Well #3 was determined by fitting the analytical solution to the experimental chlorophyll concentration data. The fitted concentration histories together with the experimental data are presented in Figure 9. The hydrodynamic dispersion coefficient used, D = 20 cm^2/d, was previously determined from chloride dilution tracer tests [*Di Fazio et al.*, 1996]. It was estimated that U = 8, 18, 6, 6, 0.5, 13 and 10 cm/d at well depths below the water table of d = 0.5, 10, 15, 20, 26, 32 and 37 m, respectively. Therefore the mean water velocity in the wellbore $\overline{U}_{wb}$ (L/t) is 8.8 cm/d. It should be noted that the observed variability in water velocity with depth, suggests the existence of independent, parallel fractures with different water flow regimes. Note that the mean water velocity in the wellbore is essentially the local specific discharge of the aquifer.

[18] For a subsurface rock formation containing N_f parallel fractures with the same mean aperture $\bar{b}$, the total volumetric flow rate per unit width of the formation Q'_x (L^2/t) is given by:

$$Q'_x = q_t B = \overline{U} N_f \bar{b} = \overline{U} n_e B \tag{7}$$

where q_t (L/t) is the formation or overall specific discharge; $\overline{U}$ (L/t) is the average water velocity in a single fracture; and $N_f\bar{b} = n_e B$ is the void volume per unit of horizontal area of the aquifer. The latter expression in the preceding relationship is a consequence of (4). The average water velocity from a single fracture is given by [*Bear*, 1972, p.14]:

$$\overline{U} = -\frac{\gamma_w}{\mu_w}\frac{\bar{b}^2}{12}\frac{\partial \phi}{\partial x} \tag{8}$$

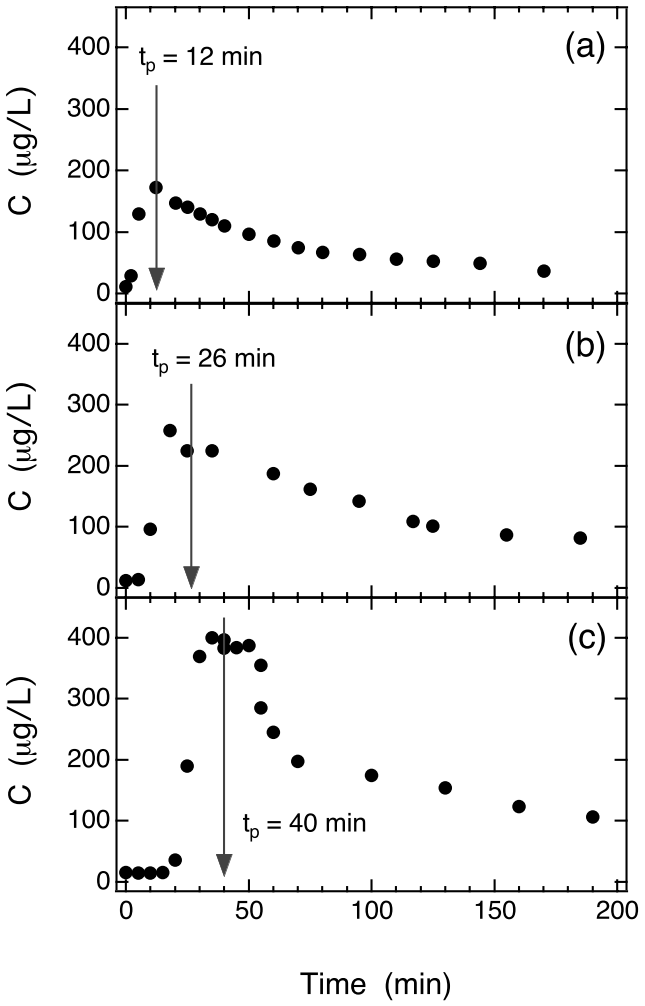

Figure 7. Iodine tracer breakthrough concentrations (solid circles) observed at well WT2 together with the corresponding estimated pumping periods (vertical solid vectors) for flow rates of (a) 112 m^3/h, (b) 50 m^3/h and (c) 25 m^3/h.

In view of (7) and (8), the mean aperture $\overline{b}$ is expressed as:

$$\overline{b} = \left(-\frac{12 q_t}{n_e} \frac{\mu_w}{\gamma_w} \frac{\partial x}{\partial \phi} \right)^{1/2} \tag{9}$$

Although the transmissivity, T (L^2/t), of a fractured rock formation is best estimated with pumping or slug tests (see next section), it can also be obtained from the following expression [*Bear*, 1993, p.15]:

$$T = \frac{Q'_x}{-\partial \phi / \partial x} = \frac{\overline{U} n_e B}{-\partial \phi / \partial x} = \frac{\gamma_w}{\mu_w} \frac{\overline{b}^2}{12} n_e B \tag{10}$$

Assuming that $q_t \approx \overline{U}_{wb}$ = 8.8 cm/d (average water velocity in the wellbore), and by employing the measured and estimated parameter values applicable for the field conditions, B = 40 m, n_e = 0.0032, $\partial\phi/\partial x$ = −0.004 [*Masciopinto et al.*, 2001], γ_w = 1000 kg/$m^2 \cdot s^2$, and μ_w = 1.16×10^{-4} kg/m · s for water at 15°C [*Weast*, 1969], the average of the mean apertures of the parallel fractures in Well #3 is evaluated from (9) to be $\overline{b}$ = 0.333 mm, and the transmissivity is estimated from (10) to be T = 0.01 m^2/s.

2.1.3. Pumping Tests

[19] A pumping test was conducted in Well #4 in order to evaluate the local aquifer transmissivity. The well was pumped with a constant volumetric flow rate of Q_w = 79.2 m^3/h, for a time period of 13 min. The water levels in the borehole were measured with a pressure probe (OTT Hydrometry, model Orpheus SN), which was positioned 1 m below the water level in the Well #4. The observed drawdown during both pumping and recovery periods are presented in Figure 10a. The following analytical solution describing the spatially and temporally dependent aquifer drawdown, s(r, t), under unsteady radial flow conditions derived by Theis can be used in conjunction with the superposition principal to obtain an expression for the residual drawdown [*Todd*, 1980, p.133]:

$$s' = \frac{2.30 Q_w}{4\pi T} \log\left(\frac{t}{t'}\right) \tag{11}$$

where s' (L) is the residual drawdown, t (t) is time since pumping started; and t' (t) is time since pumping stopped.

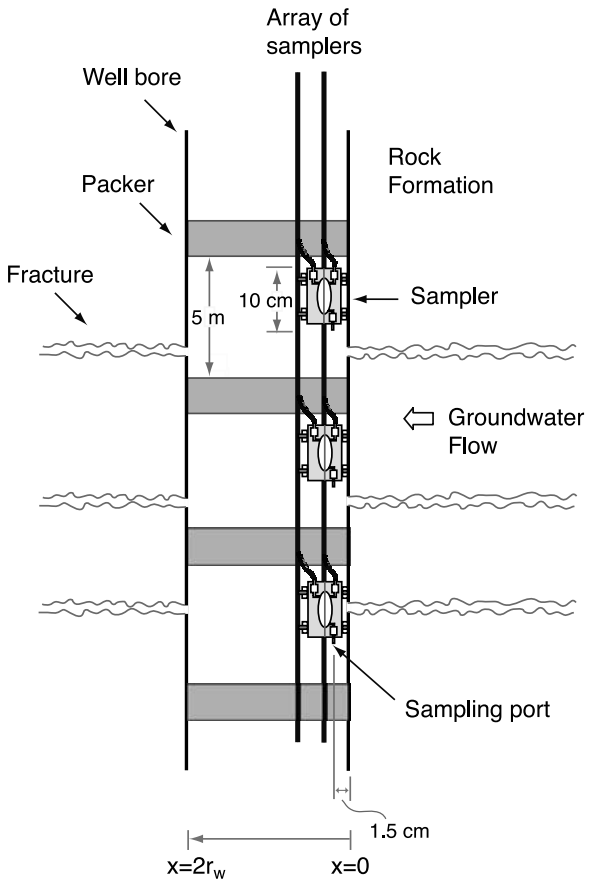

Figure 8. Illustration of a well borehole with radius r_w containing an array of three water samplers (the actual number of samplers inserted in Well #3 is 7). Each sampler is located within a 5 m section of the borehole, which is isolated by two inflatable packers. The sampling inlet ports are located 1.5 cm from the wall.

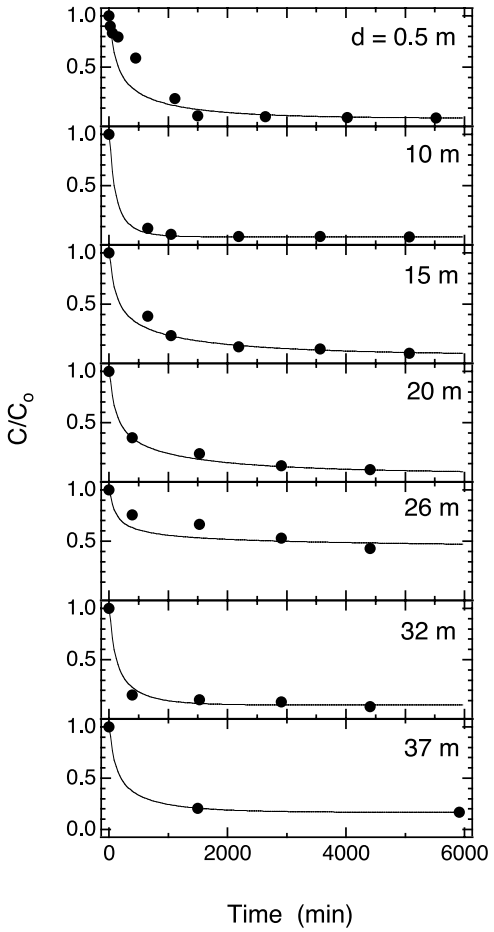

Figure 9. Observed chlorophyll concentrations at various depths below the water table in Well #3 (solid circles) and the corresponding best fitted concentration histories (solid curves). Here D = 20 cm^2/d and x = 1.5 cm.

The preceding equation is valid for r small and t′ large. A plot of s′ versus the logarithm of t/t′ forms a straight line with slope $2.30Q_w/4\pi T$. The transmissivity can be estimated from the following expression:

$$T = \frac{2.30Q_w}{4\pi\Delta s'} \tag{12}$$

where $\Delta s'$ (L) is the residual drawdown per log cycle.

[20] Figure 10b presents the residual drawdown observed in Well #4 as a function of the logarithmic ratio t/t′. The estimated residual drawdown per log cycle is $\Delta s' = 3.9$ cm. Consequently, in view of (12) the local transmissivity of the aquifer is estimated to be T = 0.10 m^2/s, which is an order of magnitude greater than the one estimated in the previous section for Well #3. This variability is attributed to the spatial heterogeneity of the Nardò fracture apertures.

[21] All other 33 pumping tests were carried out under steady radial flow at the well locations listed in Table 2. All pumping wells were fully penetrating the local saturated thickness of the aquifer. A two-hour pumping period was shown to be adequate for the achievement of steady water level in each well. The observed ratio of flowrate to drawdown at each pumping well is reported in Table 2 together with the corresponding local aquifer thickness. Furthermore, the local aquifer transmissivity at each pumping well location is determined by the Thiem equation [*Bear*, 1979; p. 306].

2.2. Fracture Aperture Spatial Variability

[22] The spatial variability of the mean fracture aperture of the Nardò aquifer can be evaluated from available local estimations of $\bar{b}$ using well-established geostatistical procedures. Tracer tests, such as the iodine tracer test (see section 2.1.1) and the chlorophyll borehole dilution tracer test (see section 2.1.2), can be used to obtain local estimates of $\bar{b}$. However, such procedures are relatively expensive and time consuming. Consequently, theoretical procedures were employed to estimate $\bar{b}$ at 33 additional observation wells within the 8400 × 7600 m^2 domain (see the area indicated by the broken line border in Figure 3). The coordinates and physical characteristics of the wells considered in the present study are listed in Table 2.

[23] In view of (1) and (4), the parameter t_p in (3) can be eliminated to yield

$$\bar{b} = \left[\frac{6Q_w}{\pi\Delta\phi n_e B}\frac{\mu_w}{\gamma_w}\log\left(\frac{r}{r_w}\right)\right]^{1/2} \tag{13}$$

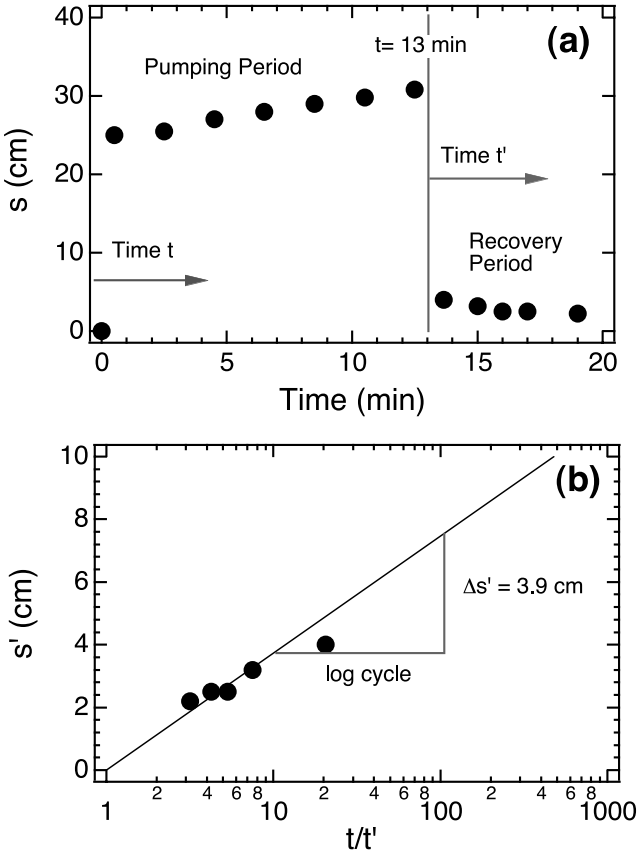

Figure 10. Results from pumping test conducted in Well #4 presented as (a) well drawdown as a function of time for both pumping and recovery periods, and (b) residual drawdown as a function of normalized time with respect to time since pumping stopped.

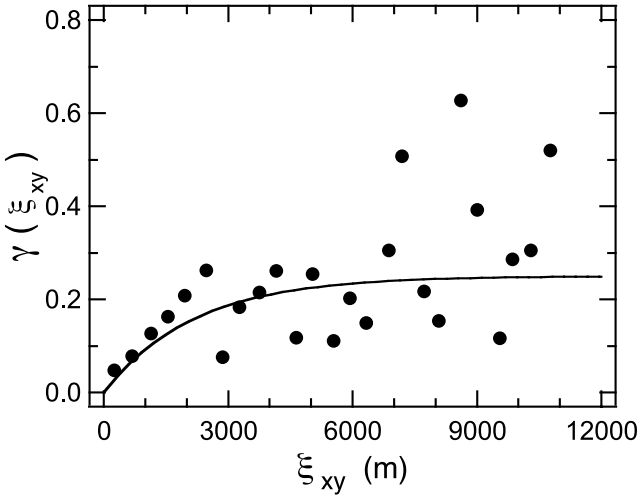

Figure 11. Experimental semi-variogram (solid circles) and fitted anisotropic semi-variogram (solid curve). Here, $\sigma_{xy}^2 = 0.25$, $\zeta_x = 1800$ m and $\zeta_y = 3000$ m.

Note that the preceding expression allows for estimation of $\overline{b}$ on the basis of known parameter values. The radius of influence during pumping is r = 220 m, as estimated by first using the observed water table drawdowns (5, 2 and 1 cm for 112, 50 and 25 m^3/h, respectively) in monitoring well WT1, which is 11.7 m from the pumping well WT2, and then linearly extrapolating to the distance where the corresponding drawdown is zero. The aquifer effective porosity, as determined by the iodine tracer test, is spatially uniform and equal to $n_e = 0.0032$. Furthermore, the local $\overline{b}$ values are estimated for all of the wells listed in Table 2.

[24] Assuming that $\overline{b}$ is a lognormally distributed function, we can define a stationary random field Y(x, y) and its mean value $\overline{Y}$ as follows:

$$Y(x,y) = \log_{10}\overline{b}(x,y) \tag{14}$$

$$\overline{Y} = E[Y] \tag{15}$$

where E[ ] is the expectation operator. Consequently, the residual

$$\varepsilon(x,y) = Y(x,y) - \overline{Y} \tag{16}$$

is also a random field. It should be noted that a random field is partially described by second-order characteristics, e.g., its mean function or expected value, and autocovariance function [*Christakos*, 1992]. Therefore the stationary stochastic random field for ε (x, y) is characterized by the mean function:

$$\mu_\varepsilon(x,y) = E[\varepsilon(x,y)] = 0 \tag{17}$$

indicating a zero-mean stochastic process, and by its autocovariance function:

$$R(\xi_{xy}) = E\left[\varepsilon(x_i,y_i)\varepsilon\left(x_j,y_j\right)\right] \tag{18}$$

representing the mutual variability between $\varepsilon(x_i, y_i)$ and $\varepsilon(x_j, y_j)$, or equivalently the mutual variability between $\varepsilon(x, y)$ and $\varepsilon\ (x + \xi_x, y + \xi_y)$, where

$$\xi_{xy} = \left[\left(x_i - x_j\right)^2 + \left(y_i - y_j\right)^2\right]^{1/2} \tag{19}$$

$$\xi_x = \left|x_i - x_j\right| \tag{20}$$

$$\xi_y = \left|y_i - y_j\right| \tag{21}$$

The autocovariance function of a stationary random field is related to the semi-variogram by [*Journel and Huijbregts*, 1978; *Isaak and Svrivastava*, 1989]

$$R(\xi_{xy}) = R(0) - \gamma(\xi_{xy}) \tag{22}$$

where $R(0) = E[\varepsilon^2(\xi_{xy})]$ is the variance of $\varepsilon(\xi_{xy})$, representing the mean square deviation of $\varepsilon\ (\xi_{xy})$ from its mean value, $\mu_\varepsilon(\xi_{xy}) = 0$, and $\gamma(\xi_{xy})$ is the semi-variogram defined as:

$$\gamma(\xi_{xy}) = \frac{1}{2}E\left[\left\{\varepsilon(x,y) - \varepsilon\left(x+\xi_x, y+\xi_y\right)\right\}^2\right] \tag{23}$$

To determine the covariance function $R(\xi_{xy})$ the data for Y(x, y) presented in Table 2 were detrended and the experimental semi-variogram of the detrended data was constructed, as illustrated by the solid circles in Figure 11. Assuming that the experimental semi-variogram can be fitted with the following two-dimensional exponential, theoretical semi-variogram model:

$$\gamma(\xi_{xy}) = \sigma_{xy}^2\left\{1 - \exp\left[\left(\frac{\xi_x^2}{\zeta_x^2} + \frac{\xi_y^2}{\zeta_y^2}\right)^{1/2}\right]\right\} \tag{24}$$

where $\sigma_{xy}^2 = R(0)$ is the variance or the sill of the log-transformed mean aperture; $\zeta_x > 0$ is the correlation length in the x-direction; and $\zeta_y > 0$ is the correlation length in the y-direction. The software *SURFER* [1999] was employed for the estimation of the unknown semi-variogram model parameters: $\sigma_{xy}^2 = 0.25$ and $\zeta_x = 1800$ m, and $\zeta_y = 3000$ m. The fitted semi-variogram model is indicated by the solid curve in Figure 11.

[25] Combining (22) and (24) yields the desired autocovariance function:

$$\begin{aligned} R(\xi_{xy}) &= \sigma_{xy}^2 \exp\left[\left(\frac{\xi_x^2}{\zeta_x^2} + \frac{\xi_y^2}{\zeta_y^2}\right)^{1/2}\right] \\ &= 0.25\exp\left[\left(\frac{\xi_x^2}{1800^2} + \frac{\xi_y^2}{3000^2}\right)^{1/2}\right] \end{aligned} \tag{25}$$

The above autocovariance function is employed for the generation of various realizations of the log transformed mean aperture distribution following the methodology presented by *Moreno et al.* [1988]. Figure 12 shows one

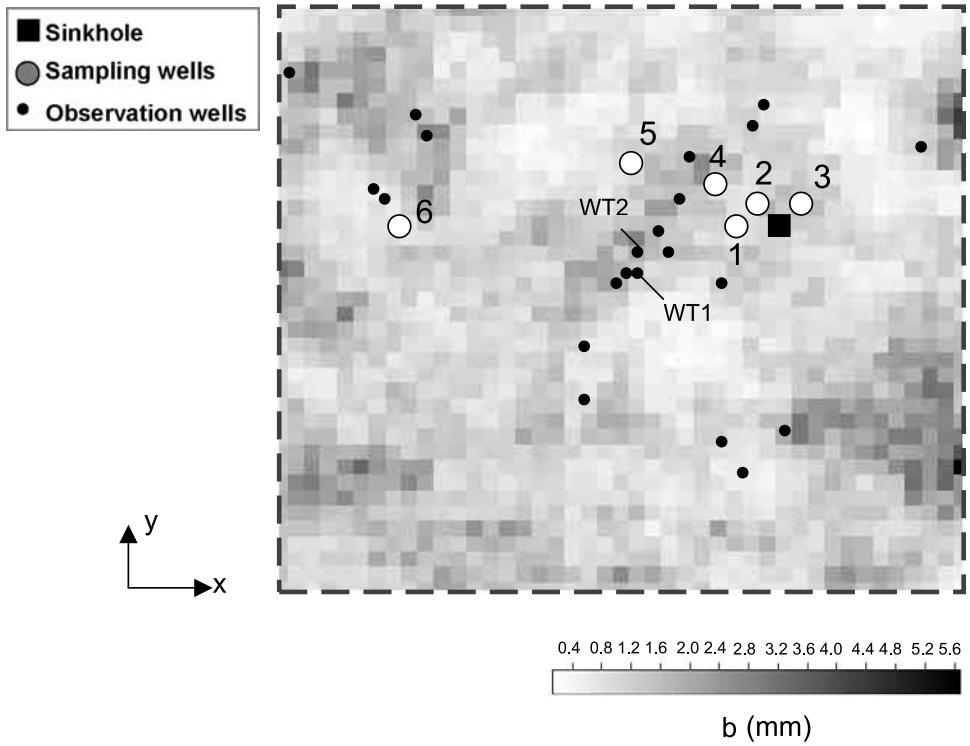

Figure 12. Schematic illustration of an aperture field realization. The domain is partitioned into 42 × 38 elements of equal size (200 × 200 m^2). The gray scale indicates the aperture sizes. (Here L_x = 8400 m; L_y = 7600 m; $\overline{b}$ = 1.072 mm; σ_{xy}^2 = 0.25; ζ_x = 1800 m; and ζ_y = 3000 m).

typical realization among many other possible realizations of the aperture spatial variability of the study area, which is indicated by the broken line border in Figure 3.

3. Laboratory Analytical Methods

3.1. Sample Preparation

[26] In order to monitor the water quality and inactivation rate of the various pathogens in the Nardò aquifer, groundwater samples were periodically collected from the 6 sampling wells and the sinkhole (see Figure 3). The various water samples were analyzed in the laboratory, where all analytical methods employed for chemical and microbiological analyses were adopted directly from *Standard Methods* [1995]. The total dissolved halo-organic compounds were detected by gas chromatography/mass spectrometry (ECS 1000 Euroglass Analytical Instruments, Delft, Holland).

[27] Somatic coliphages or bacteriophages, which are bacterial viruses commonly present in treated municipal wastewater, have been used extensively in studies of virus transport in the subsurface [*Scandura and Sobsey*, 1997; *Schijven et al.*, 2003; *Anders and Chrysikopoulos*, 2005]. Somatic coliphages are considered to be good model viruses because they behave more conservatively (sorb less) than many pathogenic viruses, and they are relatively persistent in subsurface formations. Note that pathogen concentrations in the Nardò water samples were relatively low. Consequently, to enhance the detection of coliphages and C. spores, the water samples were pretreated with the procedures outlined in the following paragraph.

[28] Each 20 L was collected in sterile plastic containers and was pre-filtered with a 10 μm polypropylene membrane (Gelman Sciences) to remove suspended solids. Coliphage particles retained on the filtration membrane were recovered by eluting the membrane for 10 min with 3% beef extract adjusted with NaOH solution at pH 9 followed by centrifugation for 30 min, as suggested by *Carducci et al.* [2003]. The supernatant from the centrifugation process was buffered and then added to the filtered water sample. Subsequently, each filtered 20 L water sample was first concentrated to 300 mL by ultrafiltration (Vivaflow 200 - Vivascience Ltd, UK) [*Lucena et al.*, 1991] and then to a final 50 mL by MiniUltrasette apparatus (Filtron Corp.). Both ultrafiltration processes employed polyethersulfone membranes (Omega series, 10,000 NMWL; Filtron Corp.) preconditioned with 3% beef extract adjusted to pH 7 to minimize coliphage adsorption onto the filter membranes [*Nupen et al.*, 1980]. After each ultrafiltration stage, coliphages were eluted from the membrane with 3% beef extract adjusted to pH 9 and loaded back to the concentrated water sample. Finally, each concentrated 50 mL water sample was buffered and stored at 4°C until the time of laboratory analysis. Note that coliphage recovery efficiency for the two-stage ultrafiltration process was estimated to be 92.4 ± 3%.

3.2. Coliphage Plaque Assays

[29] The coliphage concentrations in the concentrated 50 mL water samples were determined by the double agar layer procedure [*EPA*, 2001]. The mutant strain of *Escherichia coli C* ATCC#13706, which is nalidixic acid resistant, was utilized as host strain stock culture (i.e., host bacteria). The soft tryptic soy agar (TSA) (2.5 mL) "top agar" (0.7%) with 0.01% nalidixic acid (i.e., the antibiotic) was aseptically put into 6 tubes (2 tubes of 1 mL undiluted sample, 2 tubes with sample at 0.1 dilution ratio, and 2 tubes with sample at

0.01 dilution ratio). Each tube contained 0.5 mL of log-phase host bacteria and was placed in a 44°C water bath. The tubes were gently rolled and their contents were poured on 6 petri dishes containing 1.5% TSA (bottom agar). After incubation in a thermostatic cell at 37°C for a time period of 16–24 h, the petri dishes were examined for the presence of lyses zones which were expressed as plaque forming units (PFU/mL). The double agar assay was estimated to have a detection limit of 0.5 PFU/mL.

4. Flow and Transport Model Development

4.1. Flow Model

[30] Steady state fluid flow through a two-dimensional fracture with spatially variable aperture is governed by the following partial differential equation [*Chrysikopoulos and Abdel-Salam*, 1997]:

$$\frac{\partial}{\partial x}\left[b^3(x,y)\frac{\partial \phi(x,y)}{\partial x}\right]+\frac{\partial}{\partial y}\left[b^3(x,y)\frac{\partial \phi(x,y)}{\partial y}\right]=0 \qquad (26)$$

where x (L) is the coordinate along the fracture length; y (L) is the coordinate along the fracture width; ϕ (L) is the local piezometric head in the fracture; and b(x, y) (L) is the spatially variable fracture aperture. The preceding equation is applicable only to laminar water flow regimes. However, groundwater flow conditions beyond the laminar range can frequently occur in large apertures or cavities when pumping/injection increases the local hydraulic gradients and consequently the local water flux. Such conditions occur in the Nardò aquifer where several fractures have mean aperture greater than $\hat{b}$ = 2.0 mm.

[31] For groundwater flow conditions beyond the laminar flow range, (26) is modified as follows:

$$\frac{\partial}{\partial x}\left[\frac{b^3(x,y)}{f_{DW}(x,y)}\frac{\partial \phi(x,y)}{\partial x}\right]^{1/2}+\frac{\partial}{\partial y}\left[\frac{b^3(x,y)}{f_{DW}(x,y)}\frac{\partial \phi(x,y)}{\partial y}\right]^{1/2}=0 \qquad (27)$$

where f_{DW} is the Darcy-Weisbach frictional factor [*Bear*, 1972, p.126]. There are several procedures available in the literature for the estimation of f_{DW}. However, in the present study the following empirical relationship developed by *Masciopinto* [1999] is employed:

$$f_{DW}(x,y)=\left(15.53+\frac{105.12}{Re^{1/2}}+\frac{992.31}{Re}-\frac{300.70}{e^{Re}}\right)\frac{96}{1000} \qquad (28)$$

where, Re is the Reynolds number defined as:

$$Re=\frac{4\rho_w|U(x,y)|r_H(x,y)}{\mu_w}=2\frac{\rho_w}{\mu_w}|U(x,y)|b(x,y) \qquad (29)$$

$$|U(x,y)|=\left[U_x^2(x,y)+U_y^2(x,y)\right]^{1/2} \qquad (30)$$

(where U_x and U_y are the velocity components in the x- and y-direction, respectively); and

$$r_H(x,y)=\frac{b(x,y)}{2} \qquad (31)$$

is the approximate local hydraulic radius for fluid flow through fractures with large cross-sections (i.e., large fracture width compared to b), and ρ_w (M/L^3) is the water density. Note that for conditions of laminar flow in fractures, the frictional factor reduces to the expression f_{DW} = 96/Re [*Masciopinto*, 1999] and, in view of (8) modified for velocity components in the x and y directions, (27) and (28) are identical.

[32] For each horizontal fracture of the Nardò aquifer within the square domain indicated with broken lines on Figure 3 the steady state flow can be described by the partial differential equation (27) subject to the following boundary conditions:

$$\phi(0,y)=\phi_0 \qquad (32a)$$

$$\phi(L_{xw_i},L_{yw_i})=\phi_{w_i} \qquad (32b)$$

$$\phi(L_x,y)=\phi_L \qquad (32c)$$

$$\frac{\partial \phi}{\partial y}(x,L_y)=0 \qquad (32d)$$

$$\frac{\partial \phi}{\partial y}(x,0)=0 \qquad (32e)$$

where L_x and L_y are the dimensions of the aquifer domain in the x and y directions, respectively; and ϕ_0 and ϕ_L are the constant piezometric heads imposed at x = 0 and x = L_x, respectively, whereas ϕ_{wi} is the piezometric head imposed at the monitoring well (or sinkhole) w_i with coordinates (x = L_{xwi},y = L_{ywi}). Boundary conditions (32c) and (32d) impose that there is no water flux through the top boundary (y = L_y) and the bottom boundary (y = 0), respectively. Note that although the flow problem described by the partial differential equation (27) subject to boundary conditions (32a)–(32e) is considered at steady state, the velocity field is spatially variable and anisotropic, due to the fracture aperture spatial variability. Flow in the rock matrix is neglected because the hydraulic conductivity in the rock matrix is several orders of magnitude smaller than the hydraulic conductivity in the fractures [*Abdel-Salam and Chrysikopoulos*, 1996].

[33] For each realization of the aperture field a distribution of the piezometric heads is obtained by solving numerically the governing fluid flow equation (27) subject to boundary conditions (32a)–(32e). The numerical method of solution is based on a finite difference approach with a central difference scheme applied to a block-centered grid. The details of the numerical procedures are reported by *Masciopinto et al.* [2000]. Furthermore, for each grid node of the aquifer domain the overall groundwater discharge is determined by multiplying the local flux from a single fracture by the previously estimated number of the horizontally oriented parallel fractures (N_f = 24) of the aquifer.

4.2. Pathogen Transport Model

[34] The governing partial differential equation for the transport of pathogens in a two-dimensional fracture with

spatially variable aperture, assuming that a) the pathogens are of equal size (monodisperse); b) they deposit onto fracture surfaces but do not penetrate the rock matrix surrounding the fracture; and c) that they may undergo first-order inactivation with different inactivation rate coefficients for those suspended in the liquid phase and those deposited onto the solid matrix; is given by [*Abdel-Salam and Chrysikopoulos*, 1995b; *Sim and Chrysikopoulos*, 1995]:

$$\frac{\partial C(t,x,y)}{\partial t}+\frac{2}{b(x,y)}\frac{\partial C^*(t,x,y)}{\partial t} = \nabla \bullet [\mathbf{D} \bullet \nabla C(t,x,y) - \mathbf{U}C(t,x,y)] - \lambda(t)C(t,x,y) - \frac{2}{b(x,y)}\lambda^*(t)C^*(t,x,y) \quad (33)$$

where C* is the concentration of pathogens deposited on the fracture surfaces, expressed as mass of colloids per unit area of the fracture surface, ∇ is the two-dimensional vector gradient operator (del); $\nabla\bullet$ denotes divergence ($\nabla \bullet \mathbf{G} = \partial G_x/\partial x + \partial G_x/\partial y$ where $\mathbf{G}$ is an arbitrary two-dimensional vector); $\mathbf{D}$ is the hydrodynamic dispersion coefficient dyadic (2×2 matrix); $\mathbf{U} = [U_x(x, y), U_y(x, y)]^T$ is the velocity vector of the interstitial flow (where the exponent T denotes transpose), which is determined from the numerical solution of flow equation (27); and $\lambda(t)$ and $\lambda^*(t)$ are the pathogen time-dependent inactivation constants for suspended and deposited virus particles, respectively.

[35] The accumulation of pathogens onto the fracture surfaces is described by the following generalized mass balance expression [*Chrysikopoulos and Abdel-Salam*, 1997; *Sim and Chrysikopoulos*, 1998]

$$\frac{\partial C^*(t,x,y)}{\partial t} = r_f\frac{C(t,x,y)}{b(x,t)} - r_r C^*(t,x,y) - \lambda^*(t)C^*(t,x,y) \quad (34)$$

where r_r (t^{-1}) is the reverse pathogen deposition rate coefficient; and r_f (L^2/t) is the forward rate coefficient, defined as

$$r_f = \kappa\left[U_x^2(x,y) + U_y^2(x,y)\right]^{1/2} F(C^*) \quad (35)$$

where κ (L) is the colloid deposition coefficient, depending on several physicochemical properties of particles and collectors as well as on microscopic colloid deposition mechanisms (i.e., Brownian diffusion, van der Waals and electrostatic forces); and F(C*) (-) is the dynamic blocking function (DBF), which takes into account the effect of previously deposited particles on subsequent colloid deposition by specifying the portion of the fracture surface area available for deposition (surface exclusion effect). The DBF depends on the shape and size of the colloids, the geometry of the sorbent, flow characteristics, and the physicochemical properties of the interstitial fluid. The value of the DBF ranges between one for a fracture surface free of colloids (C* = 0) and zero for a fracture surface completely covered (monolayer) by deposited colloids.

[36] The desired expression for C* is obtained by solving (34) subject to an initial condition of zero sorbed pathogen concentration (i.e., C*(0, x, y) = 0) as

$$C^*(t,x,y) = \frac{r_f}{b(x,y)}\int_0^t C(\tau,x,y)\exp[-(r_r+\lambda^*)(t-\tau)]d\tau \quad (36)$$

where τ is a dummy integration variable.

[37] Experimental data from several batch virus inactivation studies are reasonably described by a pseudo first-order expression with a time-dependent rate coefficient as follows [*Sim and Chrysikopoulos*, 1996; *Chrysikopoulos and Vogler*, 2004; and *Anders and Chrysikopoulos*, 2006]:

$$\frac{dC(t,x,y)}{dt} = -\lambda(t)\,C(t,x,y) \quad (37)$$

where the time-dependent inactivation rate coefficient of suspended viruses is given by

$$\lambda(t) = \lambda_0 e^{-\alpha t} \quad (38)$$

where λ_0 (1/t) is the initial inactivation rate and α (1/t) is the pathogen resistivity coefficient. Furthermore, *Yates and Ouyang* [1992] suggested that

$$\lambda^*(t) = \frac{\lambda(t)}{2} \quad (39)$$

The initial and boundary conditions imposed on the two-dimensional fracture for the colloid transport model are:

$$C(0,x,y) = 0 \quad (40a)$$

$$C\left(t, L_{xw}, y_{yw}\right) = C_o \quad (40b)$$

$$\frac{\partial C(t,L_x,y)}{\partial x} = 0 \quad (40c)$$

$$-D_{xx}(x,0)\frac{\partial C(t,x,0)}{\partial y} + U_x(x,0)C(t,x,0) = 0 \quad (40d)$$

$$-D_{yy}(x,L_y)\frac{\partial C(t,x,L_y)}{\partial y} + U_x(x,L_y)C(t,x,L_y) = 0 \quad (40e)$$

where C_0 (M/L^3) is the initial pathogen concentration at the sinkhole with coordinates ($x = L_{xw}$, $y = L_{yw}$); and D_{xx} (L^2/t) and D_{yy} (L^2/t) are the hydrodynamic dispersion coefficients in the x and y directions, respectively. Condition (40a) establishes that there is no initial concentration of pathogens in the liquid phase. The constant concentration boundary condition, (40b), implies pathogen concentration continuity at the injection site (i.e., sinkhole). Equation (40c) imposes the condition that the concentration continuity is preserved at the downstream boundary. Furthermore, conditions (40d) and (40e) imply that the lower and upper boundaries of each

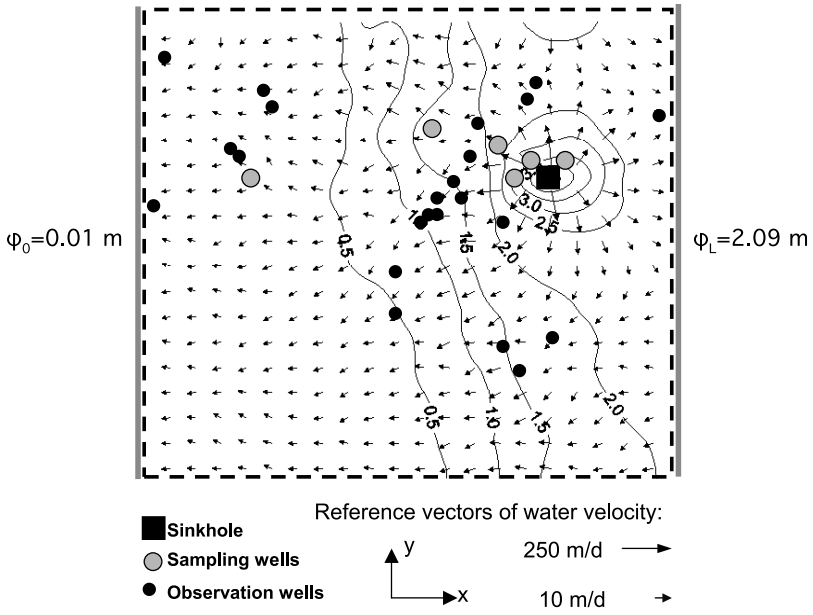

Figure 13. Piezometric head contour (in meters above sea level) during the winter of 2002 and velocity vector field in the fracture plane for a single realization of the aperture field, and the constraining piezometric heads along the upstream and downstream boundaries. The fracture is partitioned into 42 × 38 elements of equal size (200 × 200 m^2). The vector lengths are proportional to the interstitial water velocity magnitudes.

two-dimensional fracture are impervious to advective as well as dispersive transport of pathogens. The pathogen transport model (33)–(39) subject to initial and boundary conditions (40a)–(40e) is solved numerically by the fully implicit finite difference method following the procedures employed by *Chrysikopoulos and Abdel-Salam* [1997].

5. Model Simulations and Discussion

[38] The governing flow equation (27), subject to boundary conditions (32a)–(32e), was employed to estimate the piezometric head distribution and the velocity field in the Nardò aquifer. The groundwater flow model was constrained by the piezometric heads along the upstream ($x = L_x$) and downstream ($x = 0$ m) boundaries of the aquifer, which were set at $\phi_L = 2.09$ and $\phi_0 = 0.01$ m, respectively, as determined by the regional study conducted by *Cotecchia* [1977], and by the piezometric heads at the sinkhole, and Wells #1, #2, #3, and #4 as listed in Table 2. Note that the artificial water recharge into the sinkhole was assumed to be relatively constant and equal to 140 L/s, which corresponds to $\phi_w = 5.26$ m, as indicated by direct measurement of the water flow into the sinkhole during the winter of 2002. Figure 13 presents a contour plot of the piezometric head distribution in the aquifer, together with the corresponding groundwater velocity field based on the aperture field realization illustrated in Figure 12. The dominant water flow direction is oriented from East to West (from the mainland toward the Ionian Sea). The injection of the wastewater into the aquifer contributes to the development of a water table mound of about 4 m in the vicinity of the sinkhole. The vector scale in Figure 13 indicates that the magnitude of the water velocity within the aquifer ranges between 10 and 250 m/d, with an estimated average water velocity of approximately 50 m/d.

[39] The governing pathogen transport equations (33)–(39) subject to initial and boundary conditions (40a)–(40e) were employed to simulate the migration through the Nardò aquifer of the various pathogens injected at the sinkhole. The required groundwater velocity distribution was previously determined by means of the flow model. The initial concentrations of the various pathogens at the sinkhole due to the continuous injection of partially treated wastewater during the winter of 2002 are listed in Table 3. It should be noted that, although it is difficult to maintain constant the quality of the effluent water from a wastewater treatment plant, it is reasonable to assume that daily mean concentrations of the various constituents present in the partially treated wastewater remained relatively constant during the sampling period of the field experiment.

[40] The nonlinear least squares regression program PEST [*Doherty et al.*, 1994] was employed to estimate the hydrodynamic dispersion coefficients (D_{xx}, D_{yy}), the initial inactivation rate (λ_0) and the resistivity coefficient (α) by fitting the transport model to the pathogen concentrations detected at both Wells #1 and #2 during the winter of 2002. Preliminary bench scale experimentations suggested that a reasonable value for the DBF is 0.2, the deposition coefficient is $\kappa = 5 \times 10^{-6}$ m and the reverse pathogen deposition coefficient is $r_r = 0.1$ y^{-1}. The nor-

Table 3. Initial Pathogen Concentrations at the Sinkhole

Pathogen	C_0
Somatic coliphages	15,256 PFU/100mL
Clostridium Spores	1,186 CFU/100mL
Faecal coliforms	226,432 MPN/100mL
Escherichia coli	15,662 MPN/100mL
Faecal streptococci	16,090 MPN/100mL
Total bacteria	144,739 CFU/mL

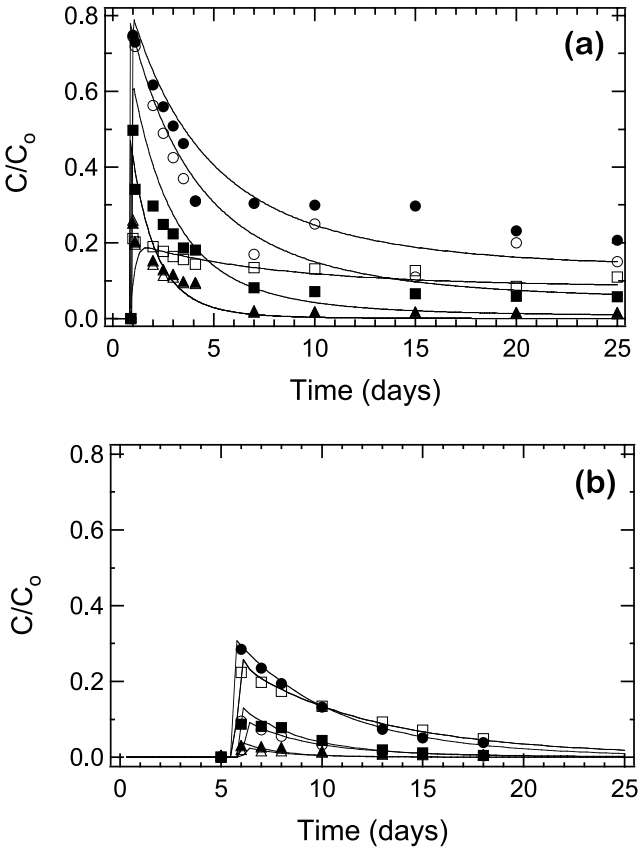

Figure 14. Normalized experimental data (symbols) and simulated concentration histories (solid curves) at (a) Well #1, and (b) Well #2. *Somatic coliphages* (open circles), *Escherichia coli* (open triangles), *faecal coliforms* (solid triangles), *fecal streptococci* (solid squares), *Clostridium spores* (open squares), total bacteria count (solid circles).

malized experimental data together with the fitted concentrations histories are shown in Figure 14. Furthermore, the fitted parameter values together with their 95% confidence intervals are listed in Table 4.

[41] The transport model was found to adequately describe the observed pathogen concentrations at both locations (Well #1 and Well #2). The normalized suspended pathogen concentrations reach a point of maximum concentration at the time of first arrival and then decrease asymptotically, mainly due to pathogen inactivation and interactions with the solid matrix. The arrival time of the various pathogens at Well #1 range from 0.9 to 1.1 days, whereas the arrival times at Well #2 range from 5.5 to 6 days. The fitted longitudinal dispersion coefficients at Wells #1 and #2, although they vary due to fracture heterogeneities and pathogen size variations, are quite similar, with a maximum difference of approximately a factor of three. The fitted transverse dispersion coefficients at Wells #1 and #2 are similar for most of the pathogens considered, but vary by an order of magnitude for *faecal coliforms* and *Escherichia coli*. These discrepancies between the fitted dispersion coefficients are attributed to field scale heterogeneities and experimental error associated with the determination of pathogen concentrations. The fitted initial inactivation rate coefficients, for the various pathogens considered, range from 0.1 to 0.9 d^{-1} (see Table 4). It should be noted that for each pathogen the fitted initial inactivation rate coefficient values remained relatively constant at the two sampling locations. This result suggests that at the two sampling locations the physicochemical conditions do not differ significantly, clearly not enough to cause any substantial change in the initial inactivation rate coefficient of the various pathogens. Furthermore, it should be noted that the fitted inactivation rate coefficient values compare well with those published in the literature for PRD1 ($\lambda = 0.48\ d^{-1}$) and MS2 ($\lambda = 1.68\ d^{-1}$) under field conditions [*Anders and Chrysikopoulos*, 2005], for PRD1 ($\lambda_0 = 0.12\ d^{-1}$) and MS2 ($\lambda_0 = 0.071\ d^{-1}$) determined from batch dynamic experiments in the presence of sand [*Anders and Chrysikopoulos*, 2006].

[42] Assuming that an acceptable setback distance is the distance traveled by a pathogen while its concentration is reduced by a 7-log [*Yates and Yates*, 1987]. The setback distance should be smaller than the distance between the source location, i.e., the sinkhole, and the point of water use. For the Nardò aquifer the corresponding time period based on the smallest initial inactivation rate ($\lambda_0 = 0.1 \pm 0.06\ d^{-1}$) listed in Table 4 is approximately 160 ± 97 days ($t_{7\text{-log}} = -\ln 10^{-7}/\lambda$). Therefore for the average groundwater velocity at the Nardò aquifer of 50 m/d, a safe setback distance of 8000 ± 4800 m is required. Note that this is the most conservative estimate and that the large uncertainty of the estimated safe setback distance is attributed to the large uncertainty of the estimated inactivation rates, which in turn are mainly due to the aquifer's heterogeneity.

6. Summary

[43] The fate and transport of pathogens that may possibly be introduced into the fractured aquifer in the Salento

Table 4. Fitted Transport Parameters

Parameter	Somatic Coliphages	Clostridium Spores	Faecal Coliforms	Escherichia Coli	Faecal Streptococci	Total Bacteria
			Well #1			
D_{xx}, m^2/y	1.35E−02 ± 3.2E−03	1.00E−02 ± 4.2E−03	1.00E−02 ± 3.8E−03	3.89E−02 ± 1.8E−02	3.48E−02 ± 6.8E−03	6.00E−02 ± 1.2E−03
D_{yy}, m^2/y	1.25E−05 ± 4.2E−06	7.84E−05 ± 3.4E−05	3.90E−04 ± 1.2E−05	2.91E−04 ± 1.1E−04	1.77E−05 ± 3.3E−06	7.13E−05 ± 3.5E−07
α, d^{-1}	0.1 ± 2.0E−03	0.1 ± 1.1E−03	0.1 ± 3.0E−03	0.1 ± 1.9E−03	0.1 ± 2.9E−03	0.12 ± 3.1E−03
λ_0, d^{-1}	0.30 ± 0.21	0.10 ± 0.06	0.90 ± 0.42	0.90 ± 0.32	0.50 ± 0.21	0.24 ± 0.06
			Well #2			
D_{xx}, m^2/y	2.01E−02 ± 0.3E−02	4.00E−02 ± 5.6E−04	1.00E−02 ± 1.2E−03	1.00E−02 ± 2.1E−03	1.00E−02 ± 4.8E−03	2.02E−02 ± 1.8E−03
D_{yy}, m^2/y	4.80E−05 ± 0.6E−05	4.82E0-5 ± 1.22E0-5	4.87E−05 ± 1.3E−06	4.87E−05 ± 4.8E−06	4.87E−05 ± 2.5E−06	6.87E−05 ± 1.1E−06
α, d^{-1}	0.05 ± 2.0E−03	0.01 ± 1.7E−03	0.01 ± 2.0E−04	0.05 ± 2.3E−03	0.01 ± 1.3E−03	0.01 ± 1.2E−03
λ_0, d^{-1}	0.43 ± 0.32	0.16 ± 0.1	0.56 ± 0.14	0.68 ± 0.21	0.33 ± 0.048	0.21 ± 0.031

(Southern Italy) during the injection of treated municipal wastewater was investigated with field scale experimentations and model simulations. All the necessary parameters required for accurate description of the aquifer were determined by two tracer tests and 34 pumping tests. The spatial variability of the mean fracture aperture was evaluated with well-established geostatistical procedures. A numerical flow model was developed to determine the distribution of the piezometric heads throughout the aquifer for each realization of the fracture aperture field. Furthermore, a finite difference transport model was developed for the simulation of pathogen migration in the fractures based on the piezometric head distributions provided by the flow model. The pathogen concentration data, collected at sampling locations Well #1 and Well #2 during the winter of 2002 were adequately fitted by the transport model. The fitted model parameters include the longitudinal and transverse coefficients, the initial inactivation rate, and the pathogen resistivity coefficient. On the basis of the slowest initial inactivation rate coefficient, the safe setback distance was estimated as being approximately 8000 ± 4800 m. This distance corresponds to a time period required by the pathogens present in the reclaimed wastewater used for the artificial aquifer recharge during the winter of 2002 to undergo at least a 7-log decrease in concentration. The estimated setback distance as well as its associated uncertainty are relatively large and suggest that in fractured aquifers, such as the Nardò aquifer, the recycled water should undergo extensive pretreatment to avoid possible waterborne disease outbreaks due to incomplete groundwater disinfection.

List of Symbols

$b(x, y)$	spatially variable aperture (L)
b_i	mean aperture of fracture i (L)
$\overline{b}$	average of the mean apertures of parallel fractures (L)
B	saturated aquifer thickness (L)
C	aqueous phase concentration (M/L^3)
C_b	background aqueous phase concentration (M/L^3)
C_0	initial aqueous phase concentration or pathogen count (M/L^3)
C*	pathogen concentration deposited on the fracture surfaces (M/L^2)
d	depth below the water table (L)
D	hydrodynamic dispersion coefficient in the water flow direction (L^2/t)
D	hydrodynamic dispersion coefficient dyadic (L^2/t)
D_{xx}	hydrodynamic dispersion coefficient in the x direction (L^2/t)
D_{yy}	hydrodynamic dispersion coefficient in the y direction(L^2/t)
E[ ]	expectation operator
f_{DW}	Darcy-Weisbach frictional factor (-)
F(C*)	dynamic blocking function (-)
g	acceleration due to gravity (L/t^2)
G	arbitrary two-dimensional vector
L_x	computational domain extent in x-direction (L)
L_y	computational domain extent in y-direction (L)
n_e	aquifer effective porosity (-)
N_f	number of horizontally oriented parallel fractures of the aquifer (-)
q_t	formation or overall specific discharge (L/t)
$\mathbf{Q'_x}$	total volumetric flow rate per unit width (L^2/t)
$\mathbf{Q_w}$	pumping flow rate (L^3/t)
r	radial coordinate distance (L)
r_f	forward deposition rate coefficient (L^2/t)
r_H	local hydraulic radius (L)
r_r	reverse deposition rate coefficient (t^{-1})
r_w	radius of the pumping well (L)
R	autocovariance function
Re	Reynolds number (-)
s	drawdown (L)
s′	residual drawdown (L)
S	aquifer storativity (-)
t	time (t)
t′	time since pumping stopped (t)
t_p	pumping period (t)
T	hydraulic transmissivity (L^2/t)
T_e	groundwater temperature (°C)
U	interstitial water velocity (L/t)
U_x, U_y	velocity components in the x- and y-direction, respectively (L/t)
U	two-dimensional interstitial water velocity vector (L/t)
$\overline{\mathbf{U}}$	average water velocity in a single fracture (L/t)
$\overline{\mathbf{U}}_{\mathbf{wb}}$	average water velocity in the wellbore (L/t)
x	Cartesian coordinate along the fracture length or flow direction (L)
y	Cartesian coordinate along the fracture width (L)
Y	lognormally distributed function, defined in (14)
$\overline{Y}$	the mean value of Y

Greek letters

α	pathogen resistivity coefficient (t^{-1})
γ	semi-variogram (-)
γ_w	specific weight of water (M/L^2t^2)
$\boldsymbol{\Delta s'}$	residual drawdown (L)
$\boldsymbol{\Delta\phi}$	piezometric head difference (L)
ε	residual equal to $Y - \overline{Y}$
ζ_x, ζ_y	correlation length in x- and y-direction, respectively (L)
$\boldsymbol{\kappa}$	colloid deposition coefficient (L)
$\boldsymbol{\lambda}$	time-dependent inactivation rate of pathogens suspended in the liquid phase (t^{-1})
$\boldsymbol{\lambda_0}$	initial inactivation constant of pathogens suspended in the liquid phase (t^{-1})
$\boldsymbol{\lambda}$*	time-dependent inactivation rate of deposited pathogens (t^{-1})
μ_w	dynamic viscosity of water (M/Lt)
ξ_x, ξ_y	separation distance between $\overline{b}$ measurements in x- and y-direction, respectively (L)
ρ_w	water density (M/L^3)
$\boldsymbol{\sigma^2}$	variance of the log-transformed mean aperture (-).

τ	dummy integration variable
ϕ	local groundwater piezometric head (L)
ϕ_w	groundwater piezometric head at an observation well or the sinkhole (L)

Abbreviations

DBF	dynamic blocking function
CFU	colony forming units
MPN	most probable number
PFU	plaque forming units
SC	specific conductance

[44] **Acknowledgments.** This research was supported by the Italian Government (Prefecture of Bari, Interior Ministry) under the 1997 Emergency Plans for public health protection of Puglia Region (Southern Italy), and by the EU under an INTERREG IIIA Greece-Italy 2000–2006 research grant. CVC was also supported in part by the Hellenic Republic Ministry of Development: General Secretariat for Research & Development under award number 05NON-EU-120.

References

Abdel-Salam, A., and C. V. Chrysikopoulos (1994), Analytical solutions for one-dimensional colloid transport in saturated fractures, *Adv. Water Resour.*, *17*, 283–296.

Abdel-Salam, A., and C. V. Chrysikopoulos (1995a), Analysis of a model for contaminant transport in fractured media in the presence of colloids, *J. Hydrol.*, *165*, 261–281.

Abdel-Salam, A., and C. V. Chrysikopoulos (1995b), Modeling of colloid and colloid-facilitated contaminant transport in a two-dimensional fracture with spatially variable aperture, *Transp. Porous Media*, *20*(3), 197–221.

Abdel-Salam, A., and C. V. Chrysikopoulos (1996), Unsaturated flow in a quasi-three-dimensional fractured medium with spatially variable aperture, *Water Resour. Res.*, *32*(6), 1531–1540.

Anders, R., and C. V. Chrysikopoulos (2005), Virus fate and transport during artificial recharge with recycled water, *Water Resour. Res.*, *41*(10), W10415, doi:10.1029/2004WR003419.

Anders, R., and C. V. Chrysikopoulos (2006), Evaluation of the factors controlling the time-dependent inactivation rate coefficients of bacteriophage MS2 and PRD1, *Environ. Sci. Technol.*, *40*(10), 3237–3242.

Bales, R. C., C. P. Gerba, G. H. Grondin, and S. L. Jensen (1989), Bacteriophage transport in sandy soil and fractured tuff, *Appl. Environ. Microb.*, *55*(8), 2061–2067.

Bales, R. C., S. R. Hinkle, T. W. Kroeger, K. Stocking, and C. P. Gerba (1991), Bacteriophage adsorption during transport through porous media: Chemical perturbations and reversibility, *Environ. Sci. Technol.*, *25*, 1088–2095.

Bear, J. (1972), *Dynamics of Fluids in Porous Media*, Elsevier.

Bear, J. (1979), *Hydraulics of Groundwater*, McGraw-Hill.

Bear, J. (1993), Modeling flow and contaminant transport in fractured rocks, Chapter 1 in *Flow and Contaminant Transport in Fractured Rock*, edited by J. Bear, C. F. Tsang and G. de Marsily, Academic Press, San Diego, California, 67–272.

Bhattacharjee, S., J. N. Ryan, and M. Elimelech (2002), Virus transport in physically and geochemically heterogeneous subsurface porous media, *J. Contamin. Hydrol.*, *57*, 161–187.

Brock, T. D., and M. T. Madigan (1991), *Biology of Microorganisms*, pp. 874, 6th ed., Prentice Hall.

Carducci, A., B. Casini, A. Bani, E. Rovini, M. Verani, F. Mazzoni, and A. Giuntini (2003), Virological control of groundwater quality using biomolecular tests, *Water Sci. Technol.*, *47*(3), 261–266.

Christakos, G. (1992), *Random Field Models in Earth Sciences*, Academic Press, San Diego, CA.

Chrysikopoulos, C. V. (1993), Artificial tracers for geothermal reservoir studies, *Environ. Geol.*, *22*, 60–70.

Chrysikopoulos, C. V., and A. Abdel-Salam (1997), Modeling colloid transport and deposition in saturated fractures, *Colloids Surf. A: Physicochem. Eng. Aspects*, *121*, 189–202.

Chrysikopoulos, C. V., and S. C. James (2002), Transport of neutrally buoyant and dense variably sized colloids in a two-dimensional fracture with anisotropic aperture, *Transp. Porous Media*, *51*, 191–210.

Chrysikopoulos, C. V., and Y. Sim (1996), One-dimensional virus transport in homogeneous porous media with time dependent distribution coefficient, *J. Hydrol.*, *185*, 199–219.

Chrysikopoulos, C. V., and E. T. Vogler (2004), Estimation of time dependent virus inactivation rates by geostatistical and resampling techniques: Application to virus transport in porous media, *Stoch. Environ. Res. Risk Assessment*, *18*(2), 67–78.

Cotecchia, V. (1977), Studies and investigations on Apulian groundwater and intruding seawaters (Salento Peninsula), *Quaderni IRSA*, *20, Rome (I)*, 145–158.

D. Lgs. 31/2 (2001), *Gazzetta Ufficiale*, Attuazione delle direttive CEE n° 80/778 concernente la qualità delle acque destinate al consumo umano, ai sensi dell'art.15, legge 16 aprile 1987 n°183.

Di Fazio, A., C. Masciopinto, and S. Troisi (1996), Prova di tracciamento con NaCl: Misura dei parametri idrogeologici e influenza della diffusione molecolare, *Groundwater Geoenginering*, *10*, 41–46.

Doherty, J., L. Brebber, and P. Whyte (1994), PEST: Model-Independent Parameter Estimation, Watermark Computing, Brisbane, Australia.

EPA (2001), Method 1601: Male-specific (F+) and Somatic Coliphage in Water by Two-step Enrichment Procedure, EPA 821-R-01-030. U.S. Environmental Protection Agency, Office of Water, Washington, D. C.

Faulkner, B. R., W. G. Lyon, F. A. Khan, and S. Chattopadhyay (2003), Modeling leaching of viruses by the Monte Carlo method, *Water Res.*, *37*, 4719–4729.

Gerba, C. P. (1984), Applied and theoretical aspects of virus adsorption to surfaces, *Adv. Appl. Microb.*, *30*, 133–168.

Harvey, R. W., and S. P. Garabedian (1991), Use of colloid filtration theory in modeling movement of bacteria through a contaminated sandy aquifer, *Environ. Sci. Technol.*, *25*, 178–185.

Hornberger, G. M., A. L. Mills, and J. S. Herman (1992), Bacterial transport in porous media: Evaluation of a model using laboratory observations, *Water Resour. Res.*, *28*(3), 915–938.

Hurst, C. J., C. P. Gerba, and I. Cech (1980), Effects of environmental variables and soil characteristics on virus survival in soil, *Appl. Environ. Microb.*, *40*, 1067–1079.

Isaak, E. H., and R. M. Svrivastava (1989), *Applied Geostatistics*, Oxford Univ. Press, Inc., New York, 308–386.

James, S. C., and C. V. Chrysikopoulos (1999), Transport of polydisperse colloid suspensions in a single fracture, *Water Resour. Res.*, *35*(3), 707–718.

James, S. C., and C. V. Chrysikopoulos (2000), Transport of polydisperse colloids in a saturated fracture with spatially variable aperture, *Water Resour. Res.*, *36*(6), 1457–1465.

James, S. C., and C. V. Chrysikopoulos (2003a), Analytical solutions for polydisperse colloid transport in uniform fractures, *Colloids Surf. A: Physicochem. Eng. Aspects*, *226*, 101–118.

James, S. C., and C. V. Chrysikopoulos (2003b), Effective velocity and effective dispersion coefficient for finite-sized particles flowing in a uniform fracture, *J. Colloid Interface Sci.*, *263*, 288–295.

James, S. C., T. K. Bilezikjian, and C. V. Chrysikopoulos (2005), Contaminant transport in a fracture with spatially variable aperture in the presence of monodisperse and polydisperse colloids, *Stoch. Environ. Res. Risk Asses.*, *19*(4), 266–279, doi:10.1007/s00477-004-0231-3.

Jewett, D. G., T. A. Hilbert, B. E. Logan, R. G. Arnold, and R. C. Bales (1995), Bacterial transport in laboratory columns and filters: Influence of ionic strength and pH on collision efficiency, *Water Res.*, *29*(7), 1673–1680.

Jin, Y., Y. Chu, and Y. Li (2000), Virus removal and transport in saturated and unsaturated sand columns, *J. Contamin. Hydrol.*, *43*, 111–128.

Journel, A. G., and C. J. Huijbregts (1978), *Mining Geostatistics*, Academic Press, London, UK.

Keswick, B. H., and C. P. Gerba (1980), Viruses in groundwater, *Environ. Sci. Technol.*, *14*(11), 1290–1297.

Knapp, R. B., M. L. Chiarappa, and W. B. Durham (2000), An experimental exploration of the transport and capture of abiotic colloids in a single fracture, *Water Res.*, *36*(11), 3139–3149.

Kurosawa, S., S. C. James, M. Yui, and M. Ibaraki (2006), Model analysis of the colloid and radionuclide retardation experiment at the Grimsel test site, *J. Colloid Interface Sci.*, *298*, 467–475.

Ledin, A., S. Karlsson, A. Duker, and B. Allard (1994), Measurements in situ of concentration and size distribution of colloidal matter in deep groundwater by photon correlation spectroscopy, *Water Res.*, *28*(7), 1539–1545.

Levenspiel, O. (1972), *Chemical Reaction Engineering*, 2nd ed., John Wiley, New York.

Liu, H. H., G. S. Bodvarrson, and L. Pan (2000), Determination of particle transfer in random walk particle methods for fractured porous media, *Water Resour. Res.*, *36*(3), 707–713.

Lucena, F., M. Divizia, E. Biziagos, J. M. Crance, A. Panà, and R. Deloince (1991), Extraction et concentration des virus des milieux hydriques, in

Virologie des milieux hydriques, Schwartzbrod L. edt, Tech. et Doc., Paris, France.

Mailloux, B. J., M. E. Fuller, T. C. Onstott, J. Hall, H. Dong, M. F. DeFlaun, S. H. Streger, R. K. Rothmel, M. Green, D. J. P. Swift, and J. Radke (2003), The role of physical, chemical, and microbial heterogeneity on the field-scale transport and attachment of bacteria, *Water Resour. Res.*, *39*(6), 1142, doi:10.1029/2002WR001591.

Masciopinto, C. (1999), Particles transport in a single fracture under variable flow regimes, *Adv. Eng. Software*, *30*(5), 327–337.

Masciopinto, C., and C. Carrieri (2002), Assessment of water quality after 10 years of reclaimed water injection: The Nardò fractured aquifer (Southern Italy), *Ground Water Monit. Rem.*, *22*(1), 88–97.

Masciopinto, C., A. Di Fazio, M. Benedini, and S. Troisi (1997), Evaluation of aquifer parameters by means of field tests and using different conceptual models, *Proc. Conference of American Soc. of Civil Eng.*, San Francisco, 493–498.

Masciopinto, C., G. Barbiero, and M. Benedini (1999), A large scale study for drinking water requirements in the Po basin (Italy), *Water International*, *24*(3), 211–220.

Masciopinto, C., M. Benedini, S. Troisi, and S. Straface (2000), Conceptual models and field test results in porous and fractured media, in *Groundwater Pollution Control*, edited by K. L. Katsifarakis, WIT Press, 245–292.

Masciopinto, C., A. Di Fazio, and S. Troisi (2001), Relation Between Experimental Data and Forecasting Models for Fractured Aquifers, *Proc. 2nd International Symposium on Protection of Groundwater from Pollution and Seawater Intrusion*, Bari (I), Futur Grafica Italia, Bari, Italy.

McCaulou, D. R., R. C. Bales, and R. G. Arnold (1995), Effects of temperature-controlled motility on transport of bacteria and microspheres through saturated sediment, *Water Resour. Res.*, *31*(2), 271–280.

McKay, L. D., R. W. Gillham, and J. A. Cherry (1993), Field experiments in a fractured clay till 2. Solute and colloid transport, *Water Resour. Res.*, *29*(12), 3879–3890.

McKay, L. D., W. E. Sanford, and J. M. Strong (2000), Field-scale migration of colloidal tracers in a fractured shale saprolite, *Ground Water*, *38*(1), 139–147.

Moreno, L., Y. W. Tsang, C. F. Tsang, V. Hale, and I. Neretnieks (1988), Flow and tracer transport in a single fracture: A stochastic model and its relation to some field observations, *Water Resour. Res.*, *24*, 2033–2048.

Nupen, E. M., N. C. Basson, and W. O. K. Grabow (1980), Efficiency of ultrafiltration for the isolation of enteric virus and coliphages from large volumes of water in studies on wastewater reclamation, *Prog. Water Technol.*, *12*, 851–863.

Oswald, J. G., and M. Ibaraki (2001), Migration of colloids in discretely fractured porous media: Effect of colloidal matrix diffusion, *J. Contamin. Hydrol.*, *52*, 213–244.

Palmer, C. D. (1993), Borehole dilution tests in the vicinity of an extraction well, *J. Hydrol.*, *146*, 245–266.

Park, N., T. N. Blanford, and P. S. Huyakorn (1992), VIRALT: A modular semi-analytical and numerical model for simulating viral transport in ground water, International Ground Water Modeling Center, Golden, CO.

Payment, P., and E. Franco (1993), Clostridium perfringens and somatic coliphages as indicators of the efficiency of drinking water treatment for viruses and protozoan cysts, *Appl. Environ. Microb.*, *59*(8), 2418–2424.

Reddy, H. L., and R. M. Ford (1996), Analysis of biodegradation and bacterial transport: Comparison of models with kinetic and equilibrium bacterial adsorption, *J. Contam. Hydrol.*, *22*, 271–287.

Rehmann, L. L. C., C. Welty, and R. W. Harvey (1999), Stochastic analysis of virus transport in aquifers, *Water Resour. Res.*, *35*(7), 1987–2006.

Reimus, P. W. (1995), The use of synthetic colloids in tracer transport experiments in saturated rock fractures, Rep. LA-13004-T, Los Alamos National Laboratory, Los Alamos, NM.

Regional Master Plan of Aqueducts (1998), PRGA, Piano Regolatore Generale degli Acquedotti, Aggiornamento. Ministero delle Infrastrutture, Final report, Bari, Italy.

Ryan, J. N., M. Elimelech, R. A. Ard, R. W. Harvey, and P. R. Johnson (1999), Bacteriophage PRD1 and silica colloid transport and recovery in an iron oxide-coated sand aquifer, *Environ. Sci. Technol.*, *33*(1), 63–73.

Scandura, J. E., and M. D. Sobsey (1997), Viral and bacterial contamination of groundwater from on-site sewage treatment system, *Water Sci. Technol.*, *35*(11–12), 141–146.

Schijven, J. F., and S. M. Hassanizadeh (2000), Removal of viruses by soil passage: Overview of modeling, processes, and parameters, *Critical Rev. Environ. Sci. Technol.*, *30*(1), 49–127.

Schijven, J. F., and J. Simunek (2002), Kinetic modeling of virus transport at the field scale, *J. Contam. Hydrol.*, *55*, 113–135.

Schijven, J. F., H. A. M. de Bruin, S. M. Hassanizadeh, and A. M. de Roda Husman (2003), Bacteriophages and clostridium spores as indicator organisms for removal of pathogens by passage through saturated dune sand, *Water Res.*, *37*, 2186–2194.

Sim, Y., and C. V. Chrysikopoulos (1995), Analytical models for one-dimensional virus transport in saturated porous media, *Water Resour. Res.*, *31*(5), 1429–1437, (Correction, *Water Resour. Res.*, 32 (5), p. 1473, 1996.)

Sim, Y., and C. V. Chrysikopoulos (1996), One-dimensional virus transport in porous media with time dependent inactivation rate coefficients, *Water Resour. Res.*, *32*(8), 2607–2611.

Sim, Y., and C. V. Chrysikopoulos (1998), Three-dimensional analytical models for virus transport in saturated porous media, *Transp. Porous Media*, *30*(1), 87–112.

Sim, Y., and C. V. Chrysikopoulos (1999), Analytical solutions for solute transport in saturated porous media with semi-infinite or finite thickness, *Adv. Water Resour.*, *22*(5), 507–519.

Smith, P. A., and C. Degueldre (1993), Colloid-facilitated transport of radionuclides through fractured media, *J. Contam. Hydrol.*, *13*, 143–166.

Standard Methods (1995), American Public Health Association, 19th Edition, Washington, D. C.

Stumm, W., and J. J. Morgan (1981), *Aquatic Chemistry*, 780 pp., 2nd ed., Wiley-Interscience.

SURFER (1999), *User Guide* Version 7, Golden Software Inc., 809 14th Street, Golden Colorado, 80401-1866.

Tim, U. S., and S. Mostaghimi (1991), Model for predicting virus movement through soils, *Ground Water*, *29*(2), 251–259.

Todd, D. K. (1980), *Groundwater Hydrology*, 2nd Edition, Wiley.

Tsang, Y. W. (1992), Usage of "equivalent apertures" for rock fractures as derived from hydraulic and tracer tests, *Water Resour. Res.*, *28*, 1451–1455.

Unice, K. M., and B. E. Logan (2000), Insignificant role of hydrodynamic dispersion on bacterial transport, *J. Environ. Eng. (ASCE)*, *126*(6), 491–500.

van der Lee, J., E. Ledoux, and G. de Marsily (1992), Modeling of colloidal uranium transport in a fractured medium, *J. Hydrol.*, *139*, 135–158.

van Genuchten, M. T., and W. J. Alves (1982), Analytical Solutions of the One-Dimensional Convective-Dispersive Solute Transport Equation, United States Dep. Of Agriculture, Technical Bulletin Number 1661, 1–149.

Vilker, V. L. (1981), Simulating virus movement in soils, in *Modeling Waste Renovation: Land Treatment*, edited by I. K. Iskandar, 223-253, Wiley.

Vilker, V. L., L. H. Frommhagen, R. Kamda, and S. Sundaram (1978), Application of ion exchange/adsorption models to virus transport in percolating beds, *AIChE Symp. Ser.*, *74*(178), 84–92.

Weast, R. C. (1969), *Handbook of Chemistry and Physics*, The Chemical Rubber Co. 18901 Cranwood Parkway, Cleveland, Ohio, 44128, F47.

Yao, K.-M., M. T. Habibian, and C. R. O'Melia (1971), Water and waste water filtration: Concepts and applications, *Environ. Sci. Technol.*, *5*(11), 1105–1112.

Yates, M. V., and Y. Ouyang (1992), VIRTUS, a model of virus transport in unsaturated soils, *Appl. Environ. Microb.*, *58*(5), 1609–1616.

Yates, M. V., and S. R. Yates (1987), A comparison of geostatistical methods for estimating virus inactivation rates in groundwater, *Water Res.*, *21*, 1119–1125.

Zhang, P., W. P. Johnson, T. D. Scheibe, K.-H. Choi, F. C. Dobbs, and B. J. Mailloux (2001), Extended tailing of bacteria following breakthrough at the Narrow Channel focus area, Uyster, Virginia, *Water Resour. Res.*, *37*(11), 2687–2698.

C. V. Chrysikopoulos, Department of Civil Engineering, University of Patras, Patras 26500, Greece. (gios@upatras.gr)

R. La Mantia and C. Masciopinto, Consiglio Nazionale delle Ricerche, Istituto di Ricerca sulle Acque Reparto di Chimica e Tecnologia delle Acque, Via Francesco De Blasio, 5, 70123 Bari, Italy. (rosanna.lamantia@ba.irsa.cnr.it; costantino.masciopinto@ba.irsa.cnr.it)